



MINISTERE DE L'ENSEIGNEMENT SUPEREUR ET DE LA
RECHERCHE SCIENTIFIQUE

Mostaganem جامعة عبد الحميد بن باديس مستغانم

Université Abdelhamid Ibn Badis

كلية العلوم و التكنولوجيا
Technologie

Faculté des Sciences et de la

DEPARTEMENT DE GENIE DES PROCEDES



N° d'ordre M2/GPM/2023

MEMOIRE DE FIN D'ETUDES DE MASTER ACADIMIQUE

Filière : Génie des procédés

Option: Génie des procédés des matériaux

Thème

Design and structural properties of novel hybrid compounds

Présenté par

ALI Faiza

Soutenu le 01/10/2023 devant le jury composé de :

Président :	MEKIBES Zohra	MCB	Université de Mostaganem
Examineur :	FARES Zineb	MAA	Université de Mostaganem
Encadrant :	CHOUAIIH Abdelkader	Professeur	Université de Mostaganem
Co-encadrant :	BOUDJENANE Fatima Zohra	Doctorante	Université de Mostaganem

Année Universitaire 2022/2023

Acknowledgements

First, I pray to Allah, the almighty, for providing me with this opportunity and granting me the capability to proceed successfully.

This work was carried out at the Laboratory of Technology and Properties of the Solid (LTPS) of the University Abdelhamid Ibn Badis of Mostaganem (UMAB).

My sincere thanks go to my supervisor, Pr Chouaih A., for having welcomed me into his laboratory, for proposing this subject, and for the trust he placed in me during this work. His unconditional support taught me a lot during my master's studies. His involvement, his help and his permanent encouragement contributed to the excellent realization of this work.

I also want to thank my co-supervisor, M^{rs}. Fatima Zohra Boudjenane, for her valuable advice and assistance. Her skills and unconditional support allowed me to learn much during my work on this thesis; working with her has been a great pleasure, and I truly appreciate her guidance. My gratitude also goes to Dr. MEKIBES Zohra for accepting to chair my thesis committee.

I also thank Miss. FARES Zineb for agreeing to examine and judge the work.

I want to express my gratitude to everyone who provided assistance, whether they were close by or distant. This includes their companionship, guidance, and backing. I appreciate all my friends for standing by me with their encouragement and positive attitude. Additionally, I'm thankful for the enjoyable times we've shared that brought smiles to my face.

And finally, thanks to my dear parents and my sister for their unwavering support throughout this journey.

Dedications

To my beloved parents

To my sister

To all those who are dear to me

Abstract:

The present work explores the DFT study of organometallic compounds based on thione molecule with the molecular formulas $C_6H_{18}N_6PtS_2.2(NO_3)$ and $C_{10}H_{26}N_6PtS_2.2(NO_3)$ with a molecular weight of 557.49, and 613.60 g/mol, respectively. Its biological activity was devoted to the existence of platinum metal linking two different thionic derivatives in the molecules. The geometric optimization was investigated through the density functional theory (DFT) utilizing the Gen and 6-311G(d, p) basis set using the Gaussian 09 software. This theory was also used for simulating molecular boundary orbital (HOMO and LUMO), Global chemical reactivity descriptors, and molecular electrostatic potential (MEP). Hydrogen bonds were confirmed by studying Hirschfield surface analysis using the Crystal Explorer software. An IR and NMR spectroscopic analysis was established using the same basis to determine the material's characteristics. The NLO study reveals the suitable materials candidature as an optoelectronic system. Finally, a molecular docking analysis was performed to test the inhibitory effect against the cyclin-dependent kinase CDK6 protein.

Keywords: DFT, organometallic compounds, Thione, MEP, NLO, Molecular docking

Résumé:

Le présent travail explore l'étude DFT de composés organométalliques à base de molécule de thione avec les formules moléculaires $C_6H_{18}N_6PtS_2.2(NO_3)$ et $C_{10}H_{26}N_6PtS_2.2(NO_3)$ avec un poids moléculaire de 557,49, et 613,60 g/mol, respectivement. Son activité biologique a été consacrée à l'existence de platine métal reliant deux dérivés thioniques différents dans les molécules. L'optimisation géométrique a été étudiée à travers la théorie fonctionnelle de la densité (DFT) en utilisant la base Gen et 6-311G(d, p) en utilisant le logiciel Gaussian 09. Cette théorie a également été utilisée pour simuler les orbitales aux limites moléculaires (HOMO et LUMO), les descripteurs de réactivité chimique globale et le potentiel électrostatique moléculaire (MEP). Les liaisons hydrogène ont été confirmées en étudiant l'analyse de surface de Hirschfield à l'aide du logiciel Crystal Explorer. Une analyse spectroscopique IR et RMN a été établie en utilisant la même base pour déterminer les caractéristiques du matériau. L'étude NLO révèle la candidature de matériaux appropriés en tant que système optoélectronique. Enfin, une analyse d'arrimage moléculaire a été réalisée pour tester l'effet inhibiteur contre la cyclin-dépendent kinase CDK6 protéine.

Mots-clés : DFT, composés organométalliques, thione, MEP, NLO, amarrage moléculaire

خالصة:

يتمثل العمل الحالي دراسة DFT للثبات ارضية المعنوية $C_{10}H_{26}N_6PtS_{2.2} (NO_3)$ و $C_6H_{18}N_6PtS_{2.2} (NO_3)$ بوزن جزيئي يبلغ 44.755 و 16.716 جم/مول على التوالي. تم تكريس تخطيط البيولوجي لوجود معن بالثنائي يربط بين التين من المشتقات التوتية المختلفة في العزلة. تم فحص التحسين الهندسي من خلال نظرية الكثافة الوظيفية (DFT) باستخدام مجموعة أسس Gen و 66-1. G (d, p) باستخدام برنامج Gaussian 09. تم استخدام هذه النظرية أي ضا ارجلة ارجلة ارجلة ارجلة (HOMO) و (LUMO) وواصفات التفاعل الكهربي العادي، والمكانت الكورسكتيكية العزلية (MEP). تم تخطيط الروابط الجزيئية من خلال دراسة تخطيط سطح هيرشفيلد باستخدام برنامج Crystal Explorer. تم إجراء تحليل طيف IR و NMR باستخدام زخم الأسس لتقدير خصائص المعدن 7 تكشف دراسة NLO عن توزيع المواد المناسبة كنظام إلكتروني ضوئي أخضر. تم إجراء تحليل الانحلال الجزيئي لتقدير الأبعاد الجزيئية ضد البروتين cyclin-dependent kinase

CDK6.

الكلمات الرئيسية: DFT ، ارجلة ارضية المعنوية، Thione MEP NLO التكملة الجزيئية

Table of contents

General introduction	2
Bibliographical references	4
Chapter I: Generalities on Thione Compounds	5
I.1. Introduction	6
I.2. Molecular structure of thione	6
I.2.1. Description of the thione structure	6
I.2.2. Thione derivatives	7
I.3. Semiconductor based on thione compounds	7
I.3.1. Definition of thione semiconductors	7
I.3.2. Physical properties of thione semiconductors	8
I.4. Area of activity of thione compounds	10
I.4.1. Biological activity	10
I.4.1.1. Molecular docking	11
I.4.2. Optoelectronic activity	12
I.4.3. Photovoltaic activity	13
I.5. Conclusion	14
Bibliographical references	15
Chapter II: Density function theory (DFT) calculations	18
II.1. Introduction	19
II.2. Time-independent density function theory	19
II.2.1. Schrodinger Hamiltonian independent of time	19
II.2.2. Hohenberg and Kohn theorems	21
II.2.3. Time-independent Kohn and Sham equations	22
II.3. Implementation of DFT	23
II.3.1. Bases of atomic orbitals	23
II.3.2. The correlation exchange functions	24
II.4. Nonlinear response theory	25
II.5. Spectral implementations of DFT	27
II.5.1. Theoretical vibrational spectra analysis	27
II.5.2. DFT methods for nuclear magnetic resonance (NMR)	30
II.6. Conclusion	31
Bibliographical references	32
Chapter III: Results and discussion	35
III.1. Introduction	36
III.2. The theoretical calculation methodology	36
III.2.1. Calculation Details	36
III.2.2. Molecular geometries studied	37
III.3. Structure description	37
III.4. IR analysis	38
III.5. Magnetic spectroscopic analysis	40
III.5.1. Magnetic spectroscopic analysis of complex 1	40
III.5.2. Magnetic spectroscopic analysis of complex 2	41

III.6. Electronic structural properties	42
III.6.1. Molecular Orbital Frontiers (FMO)	42
III.6.2. Global chemical Reactivity Descriptors	43
III.6.3. Molecular electrostatic potential analysis	45
III.7. Hirshfeld surface analysis	47
III.8. Nonlinear optical properties	50
III.9. Biological activity	52
III.9.1. Introduction	52
III.9.2. Cell lines	52
III.9.3. Molecular docking analysis	54
III.10. Conclusion	59
Bibliographical references	60
General conclusions and prospects	65

List of Figures

Figure I.1.General structure of thione.

Figure I.2.Thiones derivatives Structures.

Figure I.3.Formation of bands from MOs.

Figure I.4.Electron inter-band transitions in a direct and indirect gap semiconductor.

Figure I.5.Molecular Docking process.

Figure I.6.Form of a «Push–Pull» molecule.

Figure I.7.General scheme of charge transfer in photovoltaics.

Figure II.1.Spectral domains of electromagnetic waves.

Figure II.2.Types of vibrations.

Figure III.1.a, b Optimization of complexes 1 and 2.

Figure III.2.Representation of Molecular Orbital Frontiers of compound 1 and compound 2.

Figure III.3.Molecular electrostatic potential of complex 1 and complex 2.

Figure III.4.Hirshfeld surfaces for visualizing with d_{norm} selected the intermolecular contacts of the complexes 1 and 2.

Figure III.5.Two dimensional fingerprint plots of the complexes 1 and 2 with d_{norm} selected intermolecular contacts.

Figure III.6.Structure of Cisplatin.

Figure III.7.Binding of cisplatin moiety with deoxyribonucleic acid in DNA.

Figure III.8. (a) 3D ribbon structure of receptor/4EZ5 protein, **(b)** interaction between the active site residues of the protein and Complex 1.

Figure III.9. (a) 3D ribbon structure of receptor/4EZ5 protein, **(b)** interaction between the active site residues of the protein and Complex 2.

List of Tables

Table I.1. Biological activity of thione compounds.

Table III.1. Selected bond distances (Å) and angles (°) for 1 and 2.

Table III.2. Some influential IR. bands reveal the presence of the functional group characteristic of both complexes forms.

Table III.3. Chemical displacements of complexes 1 and 2 obtained by ¹H NMR and ¹³C NMR.

Table III.4. GCRD calculated complexes 1 and 2 values by B3LYP/6–311G(d,p).

Table III.5. Calculated molecular dipole moment (μ), polarizability (α), and first and second hyperpolarizabilities (β and γ) values for complexes 1 and 2.

Table III.6. Binding affinity and RMSD values of different poses in the 4EZ5 inhibitor of by Auto Dock 4.

Table III.7. Binding affinity and RMSD values of different poses in the 4EZ5 inhibitor of by Auto Dock 4.

Table III.8. Distance types and location of intermolecular interactions formed from the residues of the protein cyclin-dependent kinase CDK6 (PDB ID: 4EZ5) and the complex 1 and 2.

List of abbreviations and symbols

Complex (1)	trans-[Pt(NH ₃) ₂ (Imt) ₂](NO ₃) ₂
Complex (2)	trans-[Pt(NH ₃) ₂ (Me ₂ Imt) ₂](NO ₃) ₂
B3LYP	Becke 3-paramètres Lee-Yang Parr
DFT	Density Functional Theory
DMSO	Dimethylsulfoxide
FMO	Frontier Molecular Orbital
GGA	Generalized Gradient Approximation
GIAO	Gauge Independent Atomic Orbital
GTO	Gaussian Type Orbital
HOMO	Highest Occupied Molecular Orbital
IR	Infra-rouge
LDA	Local Density Approximation
LUMO	Lowest Unoccupied Molecular Orbital
MEP	Molecular Electrostatic Potential
PED	Potential Energy Distribution
NMR	Nuclear Magnetic Resonance
NLO	Nonlinear optical
STO	Slater Type Orbital
TMS	Tetramethylsilane

General Introduction

General introduction

Heterocyclic compounds containing thione has numerous practical applications in photovoltaic, optoelectronics, and biology due to its unique chemistry [1-2]. Its molecular stereochemistry is confirmed through infrared (IR) spectroscopy and nuclear magnetic resonance (NMR) spectroscopy, which can be predicted using quantum chemistry methods. These techniques save time, materials, and costs.

In silico Molecular docking is a useful method in biology, pharmacy, and medicine, as it predicts the structure of complex molecules from isolated compounds. This method is more straightforward, cheaper, and faster than in vitro experimental methods. The active sites are small molecules (ligands) that interact with a biological target (enzyme) of therapeutic interest, usually a protein (receptor), influencing the mechanism in which the protein is involved [3].

The present work proposes to study the chemical reactivity of the molecular compounds using theoretical approaches and examine the biological reactivity using molecular docking techniques. Gaussian 09 [4] software was used as a molecular modeling tool due to its computational versatility, accessibility, and ability to provide information on structural, electronic, and optoelectronic molecular properties.

This thesis is divided into three chapters. The first chapter provides a theoretical framework for exploring molecular compounds, focusing on the molecular structures and their derivatives. The second chapter introduces principles related to crystalline thione semiconductor molecular solids. The third section discusses the three domains of critical activities in these compounds: biology, photovoltaic, and optoelectronics. The fourth chapter discusses molecular docking, as both compounds have biological activity.

The second chapter outlines fundamental principles for deducing crystalline arrangements of novel molecular compounds through spectroscopic analysis methods. This chapter explores also molecular modeling using Density Functional Theory (DFT), presenting its fundamental concepts, extensions, and procedures.

General introduction

The third chapter addresses structural analysis and molecular modeling, elucidating the methodology used for theoretical calculations in diffraction. The subsequent part focuses on presenting and scrutinizing outcomes derived from molecular spectroscopic analyses on target compounds. The focus shifts to deducing the physicochemical properties of thione compounds, establishing a connection between their molecular structures and electronic/optoelectronic characteristics.

The final section delves into the molecular docking of each complex, providing a comparative analysis between them and a protein. The thesis concludes with a general conclusion and a forward-looking perspective.

Bibliographical references

- [1] T. Ozturk, E. Ertas, O. Mert, Use of Lawesson's reagent in organic syntheses, *Chem. Rev.* 107 (11), (2007), 5210–5278. <https://doi.org/10.1021/cr040650b>.
- [2] M. Patil, P. Mhaldar, V. Mahadik, D. M. Pore, Novel, green and sustainable route for synthesis of 5-aryl-4-phenyl-1,2,4-triazolidine-3-thiones, *Tetrahedron Lett* 61 (25), (2020), 152015. <https://doi.org/10.1016/j.tetlet.>
- [3] R. Chebaki, Synthèse, Caractérisation et étude computationnelle des composés hétérocycliques à intérêt biologique, (2022), Université Mohamed Khider Biskra.
- [4] M. J. Frisch, G. W. Trucks, H. B. Schlegel, G. E. Scuseria, M. A. Robb, J. R. Cheeseman, G. Scalmani, V. Barone, B. Mennucci, G. A. Petersson, H. Nakatsuji, M. Caricato, X. Li, H. P. Hratchian, A. F. Izmaylov, J. Bloino, G. Zheng, J. L. Sonnenberg, M. Hada, M. Ehara, K. Toyota, R. Fukuda, J. Hasegawa, M. Ishida, T. Nakajima, Y. Honda, O. Kitao, H. Nakai, T. Vreven, J. A. Montgomery, Jr., J. E. Peralta, F. Ogliaro, M. Bearpark, J. J. Heyd, E. Brothers, K. N. Kudin, V. N. Staroverov, R. Kobayashi, J. Normand, K. Raghavachari, A. Rendell, J. C. Burant, S. S. Iyengar, J. Tomasi, M. Cossi, N. Rega, J. M. Millam, M. Klene, J. E. Knox, J. B. Cross, V. Bakken, C. Adamo, J. Jaramillo, R. Gomperts, R. E. Stratmann, O. Yazyev, A. J. Austin, R. Cammi, C. Pomelli, J. W. Ochterski, R. L. Martin, K. Morokuma, V. G. Zakrzewski, G. A. Voth, P. Salvador, J. J. Dannenberg, S. Dapprich, A. D. Daniels, Ö. Farkas, J. B. Foresman, J. V. Ortiz, J. Cioslowski, D. J. Fox, Gaussian 09, Revision D.01 (Computer Software), Gaussian, Inc., Wallingford, CT, (2013), United States.

Chapter I

Generalities on thione compounds

I.1. Introduction:

Thione, a group of heterocyclic compounds, has garnered significant attention due to its unique chemical properties and practical applications. Thione group's presence makes it an outstanding ligand for donation in coordination chemistry [1]. The presence of these organic compounds in various aspects of our activities has become an undeniable fact that deserves attention, given their significant relevance, particularly in the invention of drugs [2-3] and the advancement of optoelectronic devices. There has been considerable interest in heterocyclic compounds in recent years due to their wide range of pharmaceutical effects. Among these compounds, five/six-membered heterocyclic compounds containing nitrogen and sulfur atoms have gained particular importance in medicinal applications. Such a combination of thione derivatives has been identified for its diverse biological activities, including antifungal, antitubercular, antibacterial, antiviral, antimicrobial, antiproliferative, and cytotoxic properties. As a result, chemists and biologists have been continuously engaged in the design and synthesis of heterocyclic hybrids, recognizing their crucial medicinal application [4].

I.2. Molecular structure of thione:

I.2.1. Description of the thione structure:

In the chemical structure of thione, the positions of carbon atoms are assumed to be at the corner(s) without explicitly showing the hydrogen atoms attached to them. It is understood that each carbon atom is bonded to enough hydrogen atoms to satisfy its valency of four bonds [5].

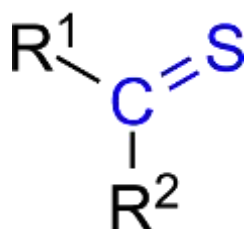


Figure I.1. General structure of thione.

I.2.2. Thione derivatives:

Sulfur-containing heterocyclic compounds, especially thiones, have significant applications in various fields, particularly medicinal chemistry and drug development. Thiones are the sulfur analogues of ketones and possess unique structural features that make them attractive for diverse biological activities [6]. Here, we present seven different classes of thiones as medicinally essential compounds that have potential biological uses, each with distinct structures:

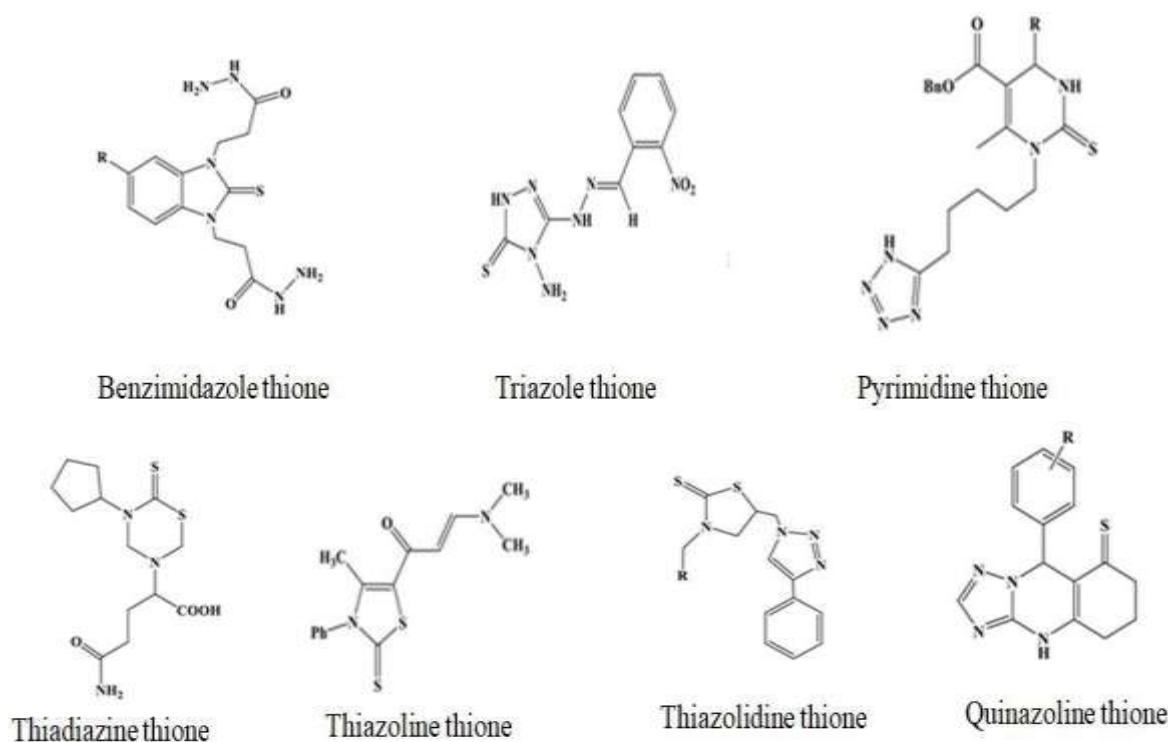


Figure I.2. Thiones derivatives Structures.

I.3. Semiconductor based on thione compounds:

The study of semiconductor thionic compounds and their properties requires basic knowledge and an overview of their fundamental concepts, which is a critical point in this chapter.

I.3.1. Definition of thione semiconductors:

Generally, organic semiconductors are divided into two categories based on their molar mass:[7]

- ✓ Organic semiconductors formed by molecules of low molar masses (small molecules) are called organic molecular semiconductors.
- ✓ Organic semiconductors formed by high molecular mass macromolecules called macromolecular semiconductors or polymers.

A molecular crystal made of thione semiconductors is an organic solid substance. It's formed by arranging conjugated thione molecules in a specific pattern and connecting them with fragile intermolecular forces [8]. These crystals have been heavily investigated to create novel, valuable materials [9]. Thione semiconductors exhibit fundamental characteristics involving the flow of electrons and holes for conduction, along with an energy gap known as a band gap [10].

I.3.2. Physical properties of thione semiconductors [11]:

Band theory explains how a solid material's ability to conduct electricity is determined by its electronic structure. In atoms, electrons are distributed into atomic orbitals based on energy levels. In molecules, multiple atomic orbitals create bonding and anti-bonding molecular orbitals (MOs), with the highest energy filled in the ground state being the Highest Occupied Molecular Orbital (HOMO). In the solid state, there are more MOs that interact, forming bands with a smaller energy gap between occupied and unoccupied bands (as depicted in Figure I.3).

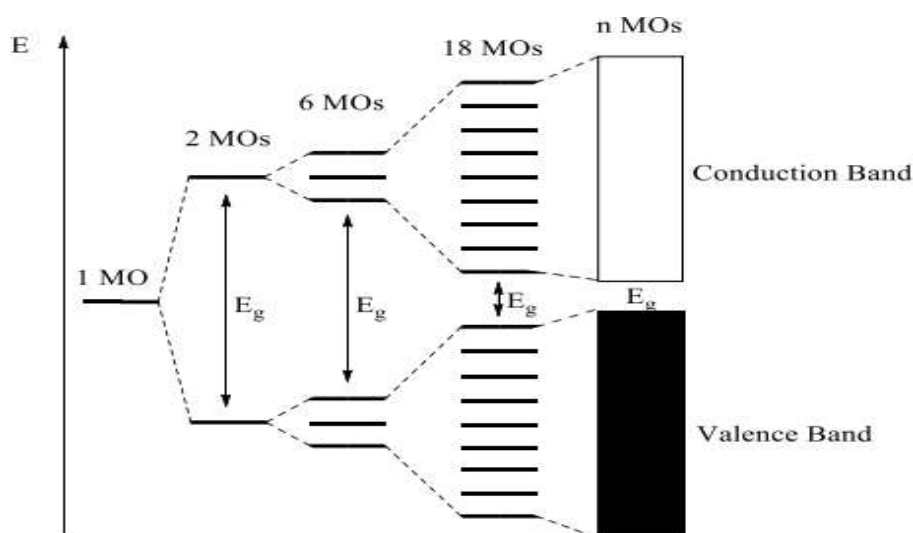


Figure I.3. Formation of bands from MOs.

The band structure in a compound is responsible for charge transfer. When atomic orbitals combine, they create molecular orbitals with two distinct energy levels. The lowest energy π

orbital is considered bonding and contributes to the valence band, while the highest energy π^* orbital is anti-bonding and contributes to the conduction band. The interaction between adjacent π orbitals facilitates charge carrier movement across the studied material [12].

The region between the molecular orbital bonds of π and the anti-bonds of π^* is called the band gap. This dimension holds significant importance in determining the classification of the material, whether it is a conductor, semiconductor, or insulator. Its width characterizes it noted E_g calculated by:

$$E_g = E_{LUMO} - E_{HOMO} \quad (\text{eq I.1})$$

This energy difference can also be described as the gap between the ionization potential (IP), the energy needed to remove an electron from the HOMO level, and the electronic affinity (EA), which is the energy required to accept an electron at the LUMO level [13].

The lowest energy of electrons in conduction and valence bands occurs at the precise energy on the abscissa scale, making a semiconductor direct. If they occur at separate momentum values, it is indirect. Indirect semiconductors require additional quasi-particles called phonons for momentum conservation. The optical absorption threshold depends on the specific band arrangement of the semiconductor material. There are two cases following the direct or indirect transition: "direct gap" semiconductors, where the upper and lower sections of the valence and conduction bands are situated at the same point in the Brillouin zone (ZB) with the same k -wave vector, and "indirect gap" semiconductors where the valence and conduction bands are situated on separate axes in the wave vector space process (refer to Figure I.4) [14].

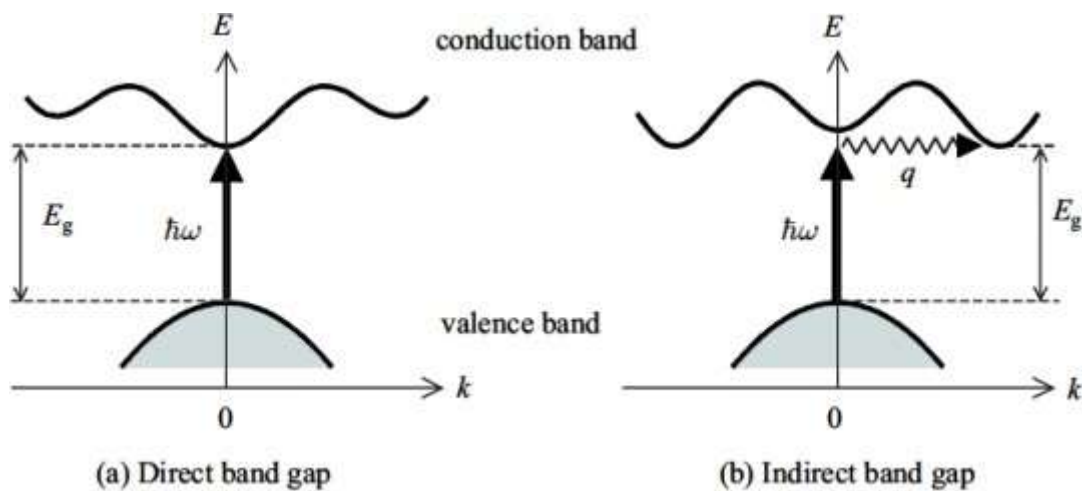


Figure I.4. Electron inter-band transitions in a direct and indirect gap semiconductor.

I.4. Area of activity of thione compounds:

Thione compounds and their derivatives have undergone extensive investigation due to their biological activities, optoelectronic capabilities, photovoltaic potential, and diverse applications across different fields.

I.4.1. Biological activity:

Thione compounds have shown promising biological properties, making them attractive for medicinal chemistry and drug discovery. They have:

- Antimicrobial activity, which can destroy or halt microorganisms, such as bacteria, fungi, and viruses[15].
- Thiones have also shown potential as anticancer agents, inducing apoptosis in cancer cells and targeting specific molecular pathways involved in cancer growth and metastasis[16].
- Antioxidant activity is another important aspect of thiones, as they effectively postpone or hinder the oxidation of substrates[17].
- Inhibitory activity against enzymes which involved in various biological processes, reducing metabolic activities within the body[18].
- Antifungal agents are compounds designed to eliminate or inhibit the growth of various fungi, with the limited number of antifungal classes due to the structural similarities between fungal and human cells[19].
- Anti-inflammatory activity is another area of interest for thione compounds. They inhibit the production of pro-inflammatory molecules and modulate immune responses, making them potential candidates for the development of anti-inflammatory drugs. Inflammation serves a beneficial role in activating the immune system to eradicate pathogens and restore damaged tissues[20].

In summary, Thione compounds have a wide range of biological activities, making them attractive for various applications in medicinal chemistry and drug discovery.

The table provided below presents several examples illustrating the biological activities linked to thione compounds, these instances demonstrate the diverse range of biological activities exhibited by thionecompounds:


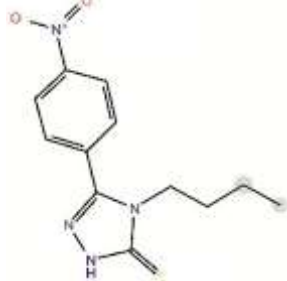
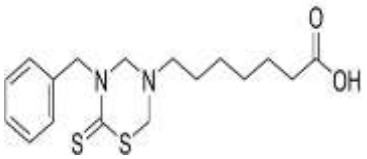
Activity	Compound	Protein	Pdb ID	Structure	References
Antiviral Activity	pyrimidine-2-thiones	main protease enzyme of SARS-CoV-2	6Y2E		[21]
Anticancer Activity	1,2,4-Triazolin-5-thione	kinase inhibitors	CK1 γ		[22]
Enzyme Inhibition	Thiadiazine-thiones	leishmania pteridine reductase	PTR1		[23]

Table I.1. Biological activity of thione compounds.

I.4.1.1. Molecular docking:

Molecular docking is a widely used technique in virtual screening strategies, primarily used for designing drugs based on the target molecule's structure. It predicts the binding position, orientation, affinity, and interaction between a small molecule (a ligand) and a biologically significant target (typically a protein) with therapeutic implications (Figure I.5). The conventional docking method was based on Fischer's lock-and-key theory, which treated both ligand and receptor as rigid systems [24]. Koshland introduced the "induced-fit" theory, accounting for the flexibility of both ligand and receptor during the docking process to enhance prediction accuracy. Understanding the molecular interactions between target and ligand is crucial for various diseases, as it helps design ligands that can either restrain or activate target proteins, influencing essential biochemical processes like signal transmission, gene transcription, and enzyme catalysis. Molecular docking methodologies offer an attractive and economical alternative to high throughput screening, which requires substantial investments in drug discovery [25].

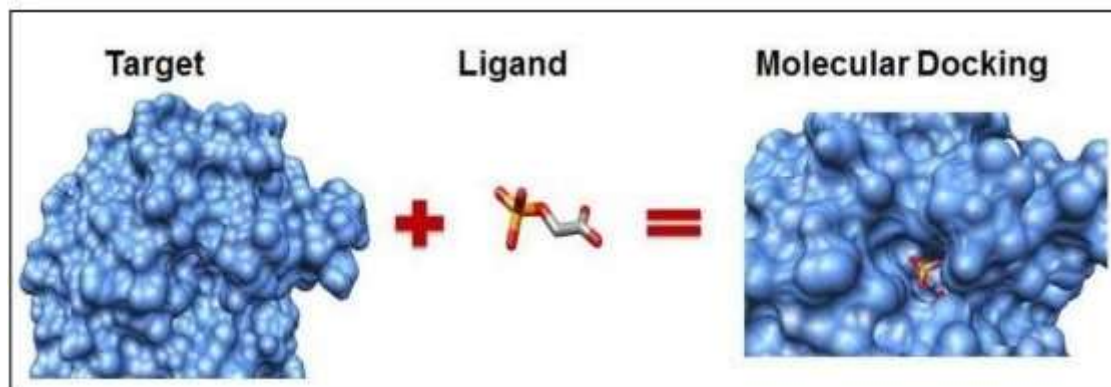


Figure I.5. Molecular Docking process.

I.4.2. Optoelectronic activity:

Crystals made from semi-organic materials exhibit a strong nonlinear optical reaction, impressive resistance to damage, minimal sensitivity to angles, and excellent mechanical and thermal stability. The crystal's lack of symmetry encourages second harmonic generation, a fundamental necessity for many contemporary electro-optical devices [26].

Thione compounds' distinctive electronic and optical properties are primarily responsible for optoelectronic behaviour.

→ Electron Donor-Acceptor Systems

Nonlinear characteristics in nonlinear optics arise from repositioning the electron system, allowing compounds to adapt to disruptions by altering their geometry. Effective molecules must have a non-centrosymmetric arrangement to have a nonzero hyperpolarizability coefficient. This category includes "push-pull" compounds, which have intramolecular charge transfer and a donor and acceptor group strategically positioned at opposite ends of a transmitting system [27].

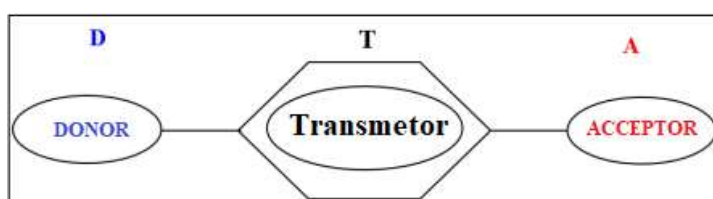


Figure I.6. Form of a «Push-Pull» molecule.

I.4.3. Photovoltaic activity:

Organic compounds, particularly those based on thione, have shown remarkable energy efficiency in various types of organic photovoltaic cells. In the active layer of organic photovoltaics (OPVs), two materials, an electron acceptor and an electron donor, are blended due to their high electron affinity and ionization potential. When an electron is excited from the donor's HOMO to the LUMO, it moves to the acceptor's LUMO if the energy of the acceptor's LUMO is lower than that of the donor's LUMO by at least a few hundred milli-electronvolts (m-eV)(Figure I.11).

The energy difference between the donor's HOMO and the acceptor's LUMO is crucial in determining the maximum voltage output (open circuit) achievable from an OPV. This voltage output is limited empirically to around 0.6 electronvolts (eV) or less than the absorber's bandgap. Therefore, the energy bandgap, which represents the difference between the LUMO and HOMO of the materials involved in absorption, plays a significant role in this context [28].

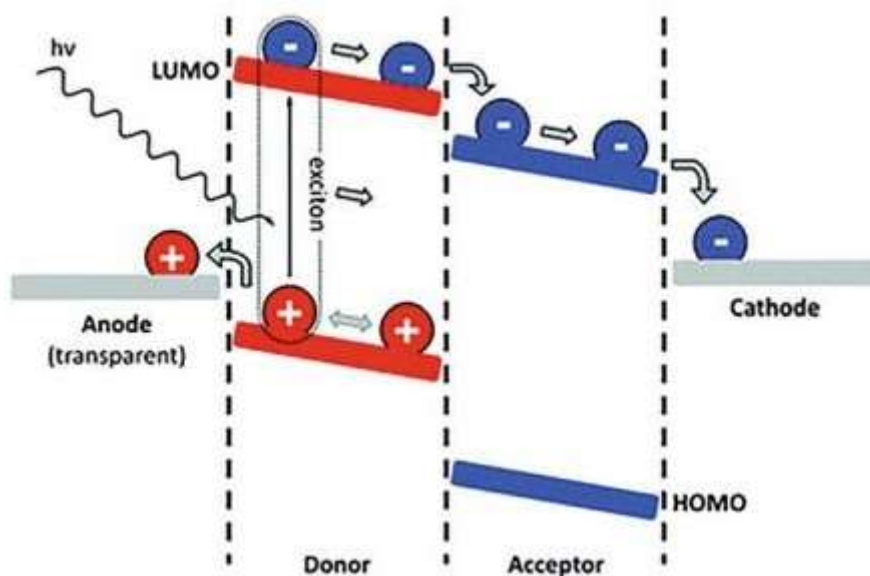


Figure I.7. General scheme of charge transfer in photovoltaics.

I.5. Conclusion:

Thione and their derivatives are important in medicine due to their various biological actions. They have antifungal, antitubercular, antibacterial, antiviral, antimicrobial, antiproliferative, and cytotoxic effects, among others. Thione show promise in biological, photovoltaic, and optoelectronic activities, opening doors for advancements in antimicrobial agents, solar cell technology, and optoelectronic devices. Studying these drugs have a high costs experimentally while Molecular docking is a technique used in virtual screening strategies to design drugs based on target molecule structure. It predicts binding position, orientation, affinity, and interaction between a ligand and a biologically significant target, with therapeutic implications. Understanding molecular interactions is crucial for diseases and offers an economical alternative to high throughput screening.

Bibliographical references:

- [1] M. Patil, P. Mhaldar, V. Mahadik, D. M. Pore, Novel, Green and Sustainable Route for The Synthesis of 5-aryl-4-phenyl-1,2,4-triazolidine-3-thiones, *Tetrahedron Lett.* 61, (2020), 25. <https://doi.org/10.1016/j.tetlet>.
- [2] D.V. Patel, N.R. Patel, *Vicinal Diaryl Substituted Heterocycles*, Elsevier, India, (2018), 245-276, ISBN: 0081022379
- [3] N. Chadha, O. Silakari, *Key Heterocycle Cores for Designing Multi targeting Molecules*, Elsevier, India, (2018), 175-209, ISBN: 9780081021057.
- [4] N. Ashokkumar, *Green Synthesis, Characterization, In-silico Molecular Docking Study and In-vitro Anticancer Activity of 1,2,3-triazolyl dihydropyrimidine-2-thione hybrids*, Master of Pharmacy in Branch-ii pharmaceutical chemistry Doctorate Thesis in pharmaceutical chemistry, (2018), Madurai medical college, Madurai.
- [5] T. S. Lobana, heterocyclic-2-thione derivatives of group 10–12 metals: coordination versatility, activation of cs (thione) bonds and biochemical potential, *coordination chemistry reviews*, (2021), 441. <https://doi.org/10.1016/j.ccr>.
- [6] A. R. Katrizky (ed.)-*Advances in Heterocyclic Chemistry*, academic press, (2007), 95. ISBN: 9780080576510
- [7] A. Moliton, *Electronique et Optoélectronique Organiques*, springer, verlag france, (2011). <https://doi.org/10.1007/978-2-8178-0103-2>.
- [8] T. U. Kampen, *Low Molecular Weight Organic Semiconductors*, wiley-vch, Germany (2010).
- [9] C. Dalinot, G. Szalóki, C. Dindault, O. Segut, L. Sanguinet, P. Leriche, *Spirobifluorene Based Small Push-Pull Molecules for Organic Photovoltaic Applications, dyes and pigments.* 140, (2017), 62-69. <https://doi.org/10.1016/j.dyepig>.
- [10] W. Brütting, *Physics of Organic Semiconductors*, Wiley-vch, Germany, (2005).
- [11] A. khaldi, *étude des propriétés optoélectroniques et mécaniques des semi-conducteurs magnétiques*, thèse de doctorat, (2019), université mohamed khider biskra.
- [12] A. Köhler, H. Bässler, *electronic processes in organic semiconductors*, wiley-vch, Germany, 1-81, (2015).
- [13] J. Fraxedas, *molecular organic materials-from molecules to crystalline solids*, Cambridge university press, 1-54, (2006).

- [14] L. Amer, L. Benbahouche, L. Imadali. simulation et analyse des propriétés et des paramètres de fonctionnement des lasers à semi-conducteurs simple et double hétérojonction algaas/gaas, mémoire de master, (2020) ,université abderahmene mira, bejaia.
- [15] R. Kirchacker, enquête de prévalence des infections nosocomiales dans une structure d'hospitalisation à domicile, thèse de doctorat en médecine, (2008), université paris des cartes (paris 5).
- [16] S. Ponnala, S. D. Prasad, iodine-mediated synthesis of 2-arylbenzoxazoles, 2-arylbenzimidazoles, and 1,3,5-trisubstituted pyrazoles. *synth. Commun*, 36, (2006), 2189. <https://doi.org/10.1080/00397910600638879>
- [17] A. K. Tiwari, antioxidants: new-generation therapeutic base for polygenic disorders, *curr.sci*, 86 (8), (2004). 1092-1102.
- [18] A. Legru, F. Verdirosa, J. F. Hernandez, G. Tassone, F. Sannio, M. Benvenuti , P. A. Conde , G. Bossis , C. A. Thomas, M. W. Crowder , M. Dillenberger, K. Becker, C. Pozzi, S. Mangani, J. D. Docquier , L. Gavara, 1,2,4-triazole-3-thione compounds with a 4-ethyl alkyl/aryl sulfide substituent are broad-spectrum metallo- β -lactamase inhibitors with re-sensitization activity. *European journal of medicinal chemistry*, (2021), 226, pp. <https://doi.org/10.1016/j.ejmech.2021.113873>
- [19] J. Yadav, B. S. Reddy, M. Srinivas, A. Prabhakar, B. Jagadeesh, Montmorillonite KSF clay-promoted synthesis of enantiomerically pure 5-substituted pyrazoles from 2,3-dihydro-4H-pyran-4-ones. *Tetrahedron Lett*, 45, (2004), 6033
- [20] A. Rykowski, D. Branowska, ring transformation of 3-halo-1,2,4-triazines with α -chlorocarbons: a novel route to pyrazoles with sulfonyl, sulfonamide and sulfonyloxy groups. *Heterocycles*. 10, 2095, (1996) .0385-5414.
- [21] D. S. E. Sayed, E. S. M. Abdel Rahim, Spectroscopic details on the molecular structure of pyrimidine-2-thiones heterocyclic compounds: computational and antiviral activity against the main protease enzyme of sars-cov-2. *bmc chemistry* 16, (2022), 82. <https://doi.org/10.1186/s13065-022-00881-3>
- [22] M. Pitucha, M. Janeczko, K. Klimek, E. Fornal, M. Wos, G. Pachuta-Stec, A. Agnieszka, kaczor, 1,2,4-triazolin-5-thione derivatives with anticancer activity as $ck1\gamma$ kinase inhibitors, *bioorganic chemistry*, 99, (2020). <https://doi.org/10.1016/j.bioorg.2020.103806>.
- [23] M. Shtaiwi, Thiadiazine-thiones as inhibitors of leishmania pteridine reductase (ptr1) target: investigations and in silico approach, *journal of biomolecular structure and dynamics*, (2023). <https://doi.org/10.1080/07391102.2023.2246589>

[24] E. Fischer, Einfluss der Configuration auf die Wirkung der Enzyme. *berdtsch chem ges*, 27, (1894), 2985–2993. <https://doi.org/10.1002/cber.18940270364>

[25] S. Kortagere, N. J. Totowa, *In silico models for drug discovery*. humana press, (2013).

[26] A. Khireddine, étude théorique des propriétés structurales et optiques des composés Organométalliques, Thèse de doctorat, (2022), université ferhat abbes de sétif.

[27] A. Chouaih, étude par diffraction des rayons x des propriétés structurales de molécules d'intérêt industriel, Thèse de doctorant, (2006), université abdelhamid ibn badis, mostaganem.

[28] I. Botiz, S. B. Darling, *Optoelectronics using block copolymers*, *Materials Today*, Volume 13, Issue 5, (2010), Pages 42-51. <https://doi.org/10.1016/S1369-7021>

Chapter II:

Density function theory (DFT) calculations

II.1. Introduction:

Molecular modeling of organic structures using quantum mechanics approximations is crucial for predicting structural and reactive behavior of studied systems. This technique complements and confirms experimental results. Computational science allows us to model, calculate, and store the characteristics of molecules analyzed by quantum mechanics methods. The Schrödinger equation and fundamental axioms of quantum physics serve as the foundation for numerical treatment of molecular species [1].

Density Functional Theory (DFT) is a powerful computational method that provides valuable insights into the electronic structure of compounds [2]. DFT offers an efficient approach by focusing on electron density, circumventing the complexity of solving the time-dependent Schrödinger equation. The Hohenberg-Kohn theorems establish a connection between electron density and external potential, forming the basis of DFT.

Ground-state properties of molecular compounds can be obtained by solving the Kohn-Sham equations, which introduce fictitious non-interacting electrons. Linear response theory is explored to understand their dynamic behavior under external perturbations. Practical implementation of DFT requires careful consideration of basis sets, such as atomic orbital and correlation exchange functions, to accurately describe electronic properties.

II.2. Time-independent density function theory:

II.2.1. Schrodinger Hamiltonian independent of time:

Throughout history, the renowned Schrödinger equation has been the basis for approximating theoretical calculations. Its application enables us to derive the total energy of a chemical system, in particular, from which all physicochemical characteristics can be determined at the quantum scale.

In the context of quantum mechanics and the non-relativistic case, the total energy of an isolated and stationary molecular system is described by the Schrödinger equation [3]:

$$H_M T_M(\vec{r}_i, \vec{R}_j) = E_M T_M(\vec{r}_i, \vec{R}_j) \quad (\text{eqII.1})$$

Where \vec{r}_i and \vec{R}_j are the spatial coordinates of electrons and nuclei ($i=1\dots N$ and $j=1\dots N$), E_M refers to the total molecular energy, T_M is the molecular wave function, and H_M is the molecular Hamiltonian.

The molecular Hamiltonian takes on the following structure for a molecular system containing n electrons and N nuclei, where they are engaged in electrostatic interaction:

$$H_M = T_N + T_e + V_{Ne} + V_{ee} + V_{NN} \text{ (eqII.2)}$$

With:

- $T_N = -\sum_{A=1}^N \frac{\hbar^2}{8\pi^2 M_A} \nabla_A^2$ kinetic energy of N nuclei;
- $T_e = -\sum_{K=1}^n \frac{\hbar^2}{2m_e} \nabla_K^2$ kinetic energy of n electrons;
- $V_{Ne} = -\sum_{A=1}^N \sum_{K=1}^n \frac{Z_A e^2}{4\pi\epsilon_0 r_{KA}}$ electron-nucleus attraction energy;
- $V_{ee} = \sum_{K=1}^n \sum_{L>K}^n \frac{e^2}{4\pi\epsilon_0 r_{KL}}$ electron-electron repulsion energy;
- $V_{NN} = \sum_{A=1}^N \sum_{B>A}^N \frac{Z_A Z_B e^2}{4\pi\epsilon_0 R_{AB}}$ nuclei-nuclei repulsion energy.

Where \hbar is the reduced Planck constant, m_e is the mass of the electron, e is the charge of the electron, M_A is the mass of the nuclei A , R_{AB} is the distance between nuclei A and nuclei B whose nuclear charges are respectively Z_A and Z_B , and ∇_K^2 represents the Laplacian of Keme electron.

Considering the Born-Oppenheimer approximation [4], which assumes that atomic nuclei are immobile, and utilizing the atomic unit system (where $\hbar = 1$, $m_e = 1$, $e = 1$, and $4\pi\epsilon_0 = 1$), the molecular Hamiltonian takes on the following form:

$$H_M = T_e + V_{Ne} + V_{ee} + V_{NN} \quad \text{(eqII.3)}$$

$$H_M = -\sum_{K=1}^n \frac{1}{2} \nabla_K^2 - \sum_{A=1}^N \sum_{K=1}^n \frac{Z_A}{r_{KA}} + \sum_{K=1}^n \sum_{L>K}^n \frac{1}{r_{KL}} + \sum_{A=1}^N \sum_{B>A}^N \frac{Z_A Z_B}{R_{AB}}$$

To simplify the notations, the expression of Hamiltonian becomes:

$$H_M = T_e + V_{ee} + V_{ext} \quad \text{(eqII.4)}$$

Where V_{ext} refers to the external potential exerted on the electrons of the molecular system.

Since it is infeasible to analytically solve the Schrödinger equation for a chemical system involving two or more electrons, various approximations in quantum mechanics have been

devised to obtain at least approximate solutions. Among these approximations, we are particularly interested in the Density Functional Theory (DFT) approach [2].

II.2.2. Hohenberg and Kohn theorems:

The Hohenberg-Kohn theorems are pivotal outcomes in Density Functional Theory (DFT), an extensively employed approach in quantum mechanics for investigating the electronic arrangement of systems with multiple electrons. The actual inception of this theory was sparked by the release of Hohenberg and Kohn's paper in 1964, which presented the two fundamental theorems of Density Functional Theory (DFT) [5]. In 1998, this theory received the prestigious Nobel Prize [6].

→ First Hohenberg-Kohn Theorem

All measurable quantities, particularly the total energy that defines the ground state of a chemical system in the presence of an external potential (which arises from atomic nuclei), can be calculated based on the electronic density of the system under investigation. Hence, the total energy of a chemical system can be described as a function of its electronic density. According to Hohenberg and Kohn, this energy is expressed by:

$$E_{HK}[\rho(\vec{r})] = F_{HK}[\rho(\vec{r})] + \int v_{ext}(\vec{r})\rho(\vec{r})d\vec{r} \quad (\text{eqII.5})$$

$F_{HK}[\rho(\vec{r})]$ is the universal functional of the density $[\rho(\vec{r})]$. This functional comprises the functional kinetic energy of electrons $T[\rho(\vec{r})]$ and functional electron-electron repulsion potential $V_{ee}[\rho(\vec{r})]$:

$$F_{HK}[\rho(\vec{r})] = T[\rho(\vec{r})] + V_{ee}[\rho(\vec{r})] \quad (\text{eqII.6})$$

→ Second Hohenberg-Kohn Theorem

The total energy representing a chemical system's fundamental state is equivalent to that system's lowest possible energy state.

$$E[\rho(\vec{r})] = \min E_{HK}[\rho(\vec{r})] \quad (\text{eqII.7})$$

The theorems formulated by Hohenberg and Kohn laid the crucial groundwork for Density Functional Theory (DFT). However, it was in 1965 that Kohn and Sham further advanced and completed the initial work proposed by Hohenberg and Kohn. They introduced a methodology to simplify the complexity of the equations, enabling the calculation of the total energy and various physicochemical properties of a chemical system using DFT. This

significant development allowed for more practical and efficient applications of DFT in studying the electronic structure and behaviour of molecules and materials.

II.2.3. Time-independent Kohn and Sham equations:

Kohn and Sham's approach introduced a novel concept within Density Functional Theory (DFT) and in the context of approximations in quantum theory. Their innovative idea involved devising an effective system that significantly advanced how quantum calculations and approximations were handled [7]. The concept revolved around envisioning an effective method comprising non-interacting particles ($V_{ee}[\rho(\mathbf{r})] = 0$) that occupy volume elements and give rise to what is known as electronic density. This electronic density mimics the behaviour of the interacting particles in the actual system. An effective potential governs these particles in the practical approach, $v_{eff}[\mathbf{r}]$, known as the Kohn and Sham potential. Consequently, the Hamiltonian of this effective system can be expressed as:

$$H_{eff} = T_{eff}[\rho(\mathbf{r})] + v_{eff}[\rho(\mathbf{r})] \quad (\text{eqII.8})$$

The unknown component in the expression for the total energy proposed by Hohenberg and Kohn (expression (II.5)) is the universal functional $F_{HK}[\rho(\mathbf{r})]$. In order to obtain the energy of the chemical system under investigation, this function needs to be modified, and Kohn and Sham successfully accomplished this task.

According to Kohn and Sham, the universal functional $F_{HK}[\rho(\mathbf{r})]$ is given by:

$$F_{HK}[\rho(\mathbf{r})] = T_{eff}[\rho(\mathbf{r})] + J[\rho(\mathbf{r})] + E_{xc}[\rho(\mathbf{r})] \quad (\text{eqII.9})$$

- $T_{eff}[\rho(\mathbf{r})]$ is the functional kinetic energy of electrons of the effective system;
- $J[\rho(\mathbf{r})]$ is the energy function of the Colombian interaction between two electronic densities;
- $E_{xc}[\rho(\mathbf{r})]$ is the exchange energy and correlation function.

According to Kohn and Sham, the function of exchange energy correlation reflects the summation of two energy differences: the first corresponds to the kinetic energy gap between the real system and the effective system ($T[\rho(\mathbf{r})]$ and $T_{eff}[\rho(\mathbf{r})]$) and the second gap is due to Colombian interaction. This magnitude is given by:

$$E_{xc}[\rho(\mathbf{r})] = T[\rho(\mathbf{r})] - T_{eff}[\rho(\mathbf{r})] + V_{ee}[\rho(\mathbf{r})] - J[\rho(\mathbf{r})] \quad (\text{eqII.10})$$

And so the total energy of the system, according to Kohn and Sham, is written in the form:

$$E_{KS}[\rho(\mathbf{r})] = T_{eff}[\rho(\mathbf{r})] + J[\rho(\mathbf{r})] + E_{xc}[\rho(\mathbf{r})] + \int v_{ext}(\mathbf{r})\rho(\mathbf{r})d\mathbf{r} \quad (\text{eqII.11})$$

Thus, minimizing as much as possible the energy of exchange-correlation inevitably leads to reducing the system's total energy under consideration. However, DFT is only practical at calculating the physicochemical characteristics in the fundamental state of systems without time dependence. Yet, it is necessary to be able to treat excited conditions, especially for chemical methods of photovoltaic activity [8].

II.3. Implementation of DFT:

II.3.1. Bases of atomic orbital:

In various approaches within quantum theory, molecular orbitals, which are ascertained through the solution of the Schrödinger equation, were predominantly formulated using atomic orbitals characterized by a collection of mathematical functions. This concept was advanced by physicist Clemens Roothaan, who expanded theoretical calculations to encompass molecular formations [9]. These mathematical functions, serving as the foundation for atomic orbitals, are classified into two main families:

- Slater STO orbitals [10].
- Gaussian GTO orbitals [11].

Gaussian-type orbitals have been the preferred choice in theoretical calculations due to their greater efficiency and simplicity [12]. When dealing with organic molecular structures, the bases developed by theoretical chemist John Pople and based on Gaussian orbitals are commonly employed [13]. These bases are represented by n-ijG (**), or n-ijkG (**). In these orbital sets, n Gaussian functions describe the internal orbitals (core orbitals), while valence orbitals are characterized by i j and ijk, respectively. Using symbols (*) indicates the number and type of polarization functions determined by the atom's weight. The first asterisk corresponds to adding d orbitals for heavy atoms, while the second asterisk corresponds to adding p orbitals for hydrogen atoms.

Aside from the utilization of atomic orbital foundations, the effectiveness of Density Functional Theory (DFT) fundamentally relies on the accurate handling of the exchange and correlation function, an energy term lacking a known analytical expression and necessitating approximation to determine the system's total energy. To address this requirement, correlation exchange functions come into play.

II.3.2. The correlation exchange functions:

The challenge in assessing Kohn-Sham techniques is establishing an exchange and correlation component applicable across all systems. Consequently, the precision of the DFT approach is contingent upon the approximation employed for this factor. Numerous approximations have surfaced to describe the exchange and correlation component, with the prominent ones being the local density approximation (LDA) [14] and the generalized gradient approximation (GGA) [15], both of which more or less effectively capture this aspect.

➤ **Approximation of local density LDA:**

This approximation represents the most basic method for representing exchange-correlation energy. It yields initial conclusive findings. Building upon the approach introduced by Kohn and Sham, the exchange-correlation energy is calculated by:

$$E_{XC}^{LDA}[\rho(\mathbf{r})] = \int_r \rho(\mathbf{r}) \varepsilon_{xc}[\rho(\mathbf{r})] d\mathbf{r} \quad (\text{eqII.12})$$

This approach involves partitioning space into infinitesimally small volume elements where the electron density remains uniform locally, referred to as the uniform gas model. The exchange-correlation energy attributed to each electron, denoted as $\varepsilon_{xc}[\rho(\mathbf{r})]$, can be segregated into two components, exchange and correlation: [14]

$$\varepsilon_{xc}[\rho(\mathbf{r})] = \varepsilon_x[\rho(\mathbf{r})] + \varepsilon_c[\rho(\mathbf{r})] \quad (\text{eqII.13})$$

With

$$\varepsilon_x^{LDA}[\rho(\mathbf{r})] = \varepsilon_x[\rho(\mathbf{r})] = -\frac{3}{4\pi} [3\pi^2 \rho(\mathbf{r})]^{1/3} \quad (\text{eqII.14})$$

The mathematical expression for exchange energy is precise (II.25), in contrast to correlation energy. Ceperley and Alder estimated the contribution of correlation energy [16]. They employed quantum Monte Carlo calculations to determine the overall energy of a uniform gas of electrons and then approximated the correlation energy by deducting kinetic energy and exchange energy [11].

➤ **Generalized Gradient Approximation (GGA):**

This approximation incorporates the gradient of the electron density, $\nabla\rho(\mathbf{r})$, into the exchange-correlation energy component. This inclusion accounts for the non-uniformity of

the actual electron density, which corresponds to cloud inhomogeneity. According to this approximation, the exchange-correlation energy is expressed as:

$$E_{XC}^{GGA}[\rho(\mathbf{r})] = \int_r \rho(\mathbf{r}) \varepsilon_{xc}[\rho(\mathbf{r}), \nabla \rho(\mathbf{r})] d_r \quad (\text{eqII.15})$$

In this approximation, the exchange energy is calculated by:

$$\varepsilon_x[\rho(\mathbf{r}), \nabla \rho(\mathbf{r})] = \varepsilon_x^{LDA}[\rho(\mathbf{r})] - \int_r F(s(\mathbf{r})) \rho^{4/3}(\mathbf{r}) d_r \quad (\text{eqII.16})$$

$$s(\mathbf{r}) = \frac{|\nabla \rho(\mathbf{r})|}{\rho^{4/3}(\mathbf{r})} \quad (\text{eqII.17})$$

$s(\mathbf{r})$ is the reduced-density gradient; this parameter indicates the system's inhomogeneity.

$F(s(\mathbf{r}))$ is a function expressed by several expressions in the literature. For example, the B88 function developed by Becke [17] gives the following indication for $F(s(\mathbf{r}))$:

$$F(s(\mathbf{r})) = \frac{\beta s^2(\mathbf{r})}{1 + 6\beta s(\mathbf{r}) \sinh^{-1} s(\mathbf{r})} \quad (\text{eqII.18})$$

The empirical parameter β is derived through calibration against precise exchange values for specific atoms.

- Hybrid functional:

These approximations are formulated through a linear amalgamation of the Density Functional Theory (DFT) and another quantum theoretical method, the Hartree-Fock method. This is why these approximations are labelled as hybrid functionals. Within this category of functions, the exchange-correlation energy is described by [12]:

$$E_{xc}^{hybride}[\rho(\mathbf{r})] = E_{xc}^{DFT}[\rho(\mathbf{r})] + a(E_x^{HF}[\rho(\mathbf{r})] - E_x^{DFT}[\rho(\mathbf{r})]) \quad (\text{eqII.19})$$

Where a is a parameter to be determined.

The most commonly used hybrid functional to calculate organic molecular structures is B3LYP [18]. The following expression gives the exchange-correlation energy using this functional:

$$E_{xc}^{B3LYP} = E_x^{LDA} + a_0 (E_x^{HF} - E_x^{LDA}) + a_x (E_x^{GGA} - E_x^{LDA}) + E_c^{LDA} + a_c (E_{xc}^{GGA} - E_{xc}^{LDA}) \quad (\text{eqII.20})$$

With $a_0 = 0.20$, $a_x = 0.72$ et $a_c = 0.81$ are three adjusted parameters.

II.4. Nonlinear response theory:

Nonlinear optical effects arise when electromagnetic fields are applied to different hardware systems, resulting in the generation of modified electromagnetic fields with altered properties

in amplitude, phase, frequency, and other physical characteristics [19]. In this study, we will analyze the nonlinear optical properties (NLO) of the compounds under investigation, including dipolar moment, polarisability (α), first-order hyperpolarisability (β), and second-order hyperpolarisability (γ), in the fourth chapter.

These characteristics stem from the dispersion of the π -electron system, enabling the compound to adapt to alterations in its geometry caused by external disturbances. This electronic structure and geometry interaction is accountable for the observed phenomenon. Molecules must possess a non-zero hyperpolarizability (β) to be helpful in nonlinear optic applications. The nonlinear reaction of an individual molecule to an electric field $E_i(\omega)$ can be expressed as a Taylor series expansion of the total induced dipole moment μ_t .

$$\mu_t = \mu_0 + \alpha_{ij}E_i + \beta_{ijk}E_iE_j + \dots$$

The total static dipole moment (μ_t), isotropic polarizability (α), and first-order hyperpolarizability tensor (β_{tot}) can be determined using the given equations, which involve the permanent dipole moment (μ_0), linear polarizability (α_{ij}), and tensor components of the first-order hyperpolarizability (β_{ijk}). By employing the x, y, and z components, we can compute the magnitudes of these properties [20]:

$$\mu = (\mu_x^2 + \mu_y^2 + \mu_z^2)^{\frac{1}{2}} \quad (\text{eq II.21})$$

$$\alpha = \frac{1}{3}(\alpha_{xx} + \alpha_{yy} + \alpha_{zz}) \quad (\text{eq II.22})$$

$$\beta_{tot} = (\beta_x^2 + \beta_y^2 + \beta_z^2)^{\frac{1}{2}} \quad (\text{eq II.23})$$

For the first order hyperpolarizability estimation, the detailed relation is as follows:

$$\beta_{tot} = [(\beta_{xxx} + \beta_{xyy} + \beta_{xzz})^2 + (\beta_{yyy} + \beta_{yzz} + \beta_{yxx})^2 + (\beta_{zzz} + \beta_{zxx} + \beta_{zyy})^2]^{\frac{1}{2}} \quad (\text{eq II.24})$$

The average (or absolute value) of static second-order hyperpolarizability can be simplified via the Kleinman [21] approach and computed through the expression:

$$= \frac{1}{5}(xxxx + yyyy + zzzz + 2xxyy + 2xxzz + 2yyzz) \quad (\text{eq II.25})$$

The determination of a crystalline structure is based on two methods: experimental analysis by different devices and theoretical study by molecular modeling, thanks to the development of the computer tool. Analytical techniques, nuclear magnetic resonance (NMR) and infrared (IR) are complementary. NMR lets us know the atoms' positions and infrared function groups

present in the molecules. Even if the NMR has made enormous progress in recent decades, especially with the help of pulsed to Fourier transform, infrared sometimes remains the only way to remove ambiguities that may remain as to the structure of a molecule [22].

II.5. Spectral implementations of DFT:

Density functional theory (DFT) has become a crucial tool in computational chemistry, particularly in spectroscopic analysis of chemical entities. DFT calculations are essential for predicting frequencies and spectral intensities, which are crucial for interpreting experimental spectra of complex molecules. Advancements in DFT approaches have made them accessible in quantum-chemical computational programs. DFT practices are now used for calculating molecular and electronic structures of ground-state systems and various spectral parameters related to NMR, ESR, UV-Vis, and IR [23].

Theoretical computation of vibrational frequencies is essential for experimental spectroscopists, especially in problematic and uncertain cases. The HF method, previously used, has been found to miscalculate these frequencies due to inadequate handling of electron correlation and anharmonicity of vibrations. DFT has largely overcome these errors, allowing for the calculation of optimized geometry, IR intensities, vibrational frequencies, and Raman scattering activities using different density functional approaches [24].

II.5.1. Theoretical vibrational spectra analysis:

Vibrational spectroscopy is a widely used analytical tool in various fields, primarily for the qualitative association of bands with specific structures or chemical groups. It differs from nuclear magnetic resonance, where nuclear spin is linked to one peak or multiplet. In vibrational spectra, all nuclei in a sample move together, leading to observed bands. There are a maximum of $3N-6$ experienced fundamental bands for N nuclei, and the matrix of internuclear force interactions has exclusive terms for $3N-6(3N-5)/2$. The influence of vibrational spectroscopy is evident in various fields, as it allows for the identification of bands that are not actually seen, such as overtones, combination bands, and nonconformities from the harmonic approximation. The problem of extracting force constants from vibrational frequencies remains an open one in mathematics [25]. The problem of computing the potential energy surface of the ground state can be solved by discovering efficient codes. DFT methods accurately compute ground state characteristics and potential energies, enabling them to accurately calculate vibrational spectra from the ground up. DFT models accurately

characterize bonding and provide high absolute frequencies compared to experimental values. The limitations of harmonic approximation often cause divergence between theory and experiment. DFT approaches offer high accuracy in normal mode computations, but anharmonicity and hydrogen bonding, which produce lower frequencies than harmonic approximation, may cause inconsistencies. Expanding the approach to molecular interactions could help address these issues [26].

Vibrational modes that do not involve a changing dipole moment (such as symmetrical stretching modes) do not absorb infrared radiation and are, therefore, not observed in infrared spectra. The number of fundamental vibrations in a molecule depends on the number of atoms and molecules symmetry. Diatomic molecules have one fundamental vibration, while triatomic molecules have three. Larger molecules can have multiple fundamental vibrations, including different types of stretching and bending modes.

Atomic bonds vibrate through stretching and bending vibrations. Stretching vibrations change bond length, with two types: asymmetric and symmetric. Bending vibrations change bond angle, with pitch differences of $\pm 0.5^\circ$. Bonds can rock or bend within or outside the shared plane, with a pitch difference of $\pm 0.5^\circ$ [27]. Symmetric stretch occurs when two atoms move in the same direction, causing a significant change in the molecule's dipole moment. In contrast, asymmetric stretch occurs when the atoms move in opposite directions, resulting in a minor change. The dipole moment is proportional to the distance between charges and their magnitude. Symmetric stretch results in a significant change in the dipole moment due to the increased distance between charges.

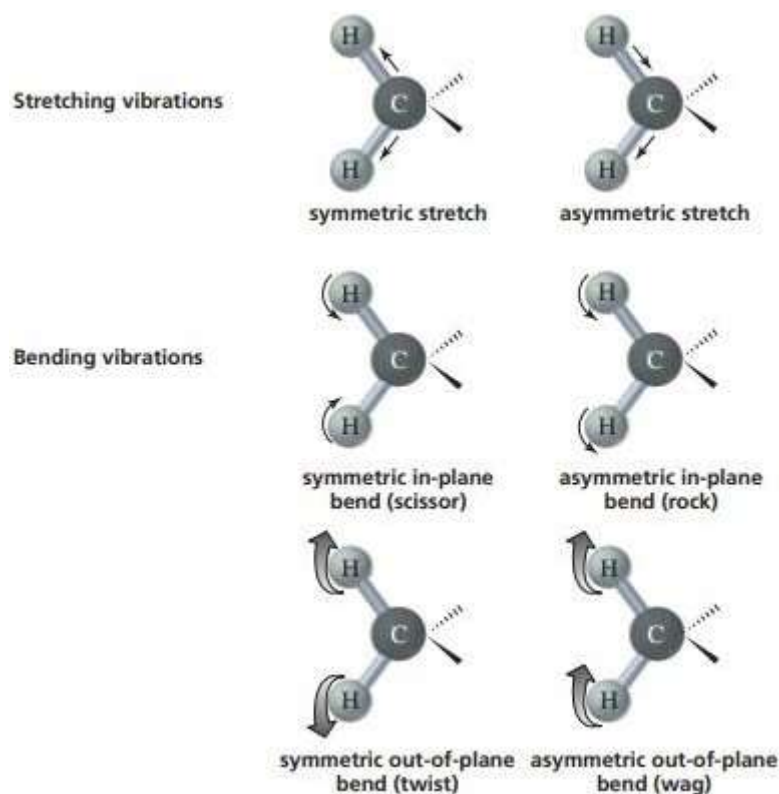


Figure II.2.Types of vibrations.

In addition to stretching and bending vibrations, which were mentioned earlier, there are four types of bending vibrations: Wagging, Scissoring, Rocking and Twisting. Each of the vibrations would absorb different frequencies of the IR. These types of molecular vibrations that can affect the dipole moment: [28]

1. **Rocking:** In a rocking vibration, the atoms in a molecule move back and forth, changing the angle between them. This can lead to a change in the dipole moment of the molecule.
2. **Scissoring:** In a scissoring vibration, the atoms in a molecule move in opposite directions, causing the angle between them to change. This can also lead to a change in the molecule's dipole moment.
3. **Twisting:** In a twisting vibration, the atoms in a molecule rotate around a bond axis, causing the molecule to change its shape. This can lead to a change in the dipole moment of the molecule.
4. **Wagging:** In a wagging vibration, the atoms in a molecule move back and forth, changing the angle between them, similar to a rocking vibration. This can also lead to a change in the molecule's dipole moment.

Each of these types of vibrations can be observed in the infrared spectrum of a molecule, providing valuable information about the structure and properties of the molecule.

A photon of light with a frequency in the infrared range will be absorbed if the bonds between atoms in the target material allow these atoms to vibrate at this frequency [29].

II.5.2. DFT methods for nuclear magnetic resonance (NMR):

In the presence of an external stationary magnetic field, the energy of a system containing nuclear or electron magnetic moments generated from the spin of a particle relies on the direction of the magnetic moment with regard to the external field. By using an oscillating external magnetic field as a probe, one can detect the energy difference for different directions of the electronic magnetic moment (electronic Zeeman effect) or nuclear magnetic moment (nuclear Zeeman effect) [30].

NMR parameters, including determined shifts, indirect spin-spin coupling constants, and direct dipole-dipole coupling constants, are linked to local and global geometry, influenced by internal flexibility and intramolecular interactions. Chemical shifts and spin-spin coupling constants are discovered as an average in experiments, but chemical shifts are often dependent on internal dynamics or intermolecular interactions. Most experimental NMR approaches rely on coupling constants or the nuclear Overhauser effect for structural information. Ab initio calculations offer insight into structure-chemical shifts or spin-spin coupling constant relationships, making data interpretation easier [31].

Various wave function tactics are limited to small and medium-sized systems, but with advancements in density functional approaches, relevant results can be obtained for larger molecules like protein and nucleic acid fragments [32]. Electron correlation effects are indirectly used in Spectral Calculations with DFT through the exchange-correlation functional. Over the past decade, DFT-based NMR computations have rapidly increased (<http://dx.doi.org/10.5772/intechopen.71080>). Methods have quickly become part of the conventional arsenal of quantum chemistry since the publication of these results. As theoretical portrayal of NMR chemical shifts based on the more conventional ab initio approaches has seen a marvelous progress as well, more thorough, technical, as well as more general evaluations are accessible [33]. Density functional theory (DFT) has recently been shown to be a viable alternative to the established Hartree-Fock (HF) and post-HF approaches for NMR calculations [34]. A very recent area of application for DFT is the inclusion of electron correlation effects in a very effective manner to determine NMR parameters.

II.6. Conclusion:

Density functional theory is a method used to calculate the energy of the state fundamental in realistic models of materials and their surfaces. The reliability of these calculations is determined by approximations for the exchange-correlation energy functional. Recent years have seen significant improvements in the quality of exchange-correlation functions, with local density gradients, density measurements, and exchange functions being introduced. The local density approximation LDA is reliable for structure, elastic modules, and phase stability but less accurate for binding energies and energy surface details far from equilibrium geometries. GGA, and hybrids retain and improve the length description of the LDA. These functions can reproduce elastic modules and vibration frequencies at less than 10%. Density functional theory (DFT) is a crucial tool in computational chemistry, particularly in spectroscopic analysis of chemical entities. It helps predict frequencies and spectral intensities, interpreting experimental spectra of complex molecules. DFT practices are used for calculating molecular and electronic structures, spectral parameters, and vibrational frequencies, overcoming errors in the HF method.

Bibliographical references

- [1] J. Götschl, Erwin Schrödinger's World View-The Dynamics of Knowledge and Reality, Springer, New York, (1992).
- [2] N. E. H. Belkafouf, Analyse structurale et spectroscopique de nouveaux matériaux fonctionnels, Thèse de doctorat, (2019), Université Abdelhamid Ibn Badis de Mostaganem.
- [3] E. Schrödinger, An undulatory theory of the mechanics of atoms and molecules, Physical Review. 28, (1926), 1049-1070. <https://doi.org/10.1103/PhysRev.28.1049>
- [4] M. Born, R. Oppenheimer, Zurquanten theorie der molekeln, Annalen der Physik. 389, (1927), 457-484. <https://doi.org/10.1002/andp.19273892002>
- [5] P. Hohenberg, W. Kohn, Inhomogeneous electron gas. Physical Review. 136, (1964), B864-B871. <https://doi.org/10.1103/PhysRev.136.B864>
- [6] M. V. Putz, Quantum Theory: Density, Condensation, and Bonding, CRC Press, Toronto, (2013), 272p. ISBN 9781774632031
- [7] W. Kohn, L. J. Sham: Self-consistent equations including exchange and correlation effects. Physical Review. 140, (1965), A1133-A1138.
- [8] H. Antaya, Design de nouvelles fonctionnelles en théorie de la fonctionnelle de la densité et conception de polymères pour application à la photovoltaïque organique, Thèse de doctorat, (2014), Université de Montréal.
- [9] C. C. J. Roothaan, New developments in molecular orbital theory, Reviews of Modern Physics, 23, (1951), 69-89. <https://doi.org/10.1103/RevModPhys.23.69>
- [10] J. C. Slater, Atomic shielding constants, Physical Review, 36, (1930), 57-64.
- [11] W. J. Hehre, R. F. Stewart, J. A. Pople, Self-consistent molecular-orbital methods, I. Use of Gaussian expansions of Slater-type atomic orbitals, The Journal of Chemical Physics.51, (1969), 2657-2664. <https://doi.org/10.1063/1.1672392>
- [12] E. Brémond, Simulation ab initio de spectres UV-visibles, Thèse de doctorat, (2012), Université Pierre et Marie Curie - Paris VI.
- [13] W. J. Hehre, R. Ditchfield, J. A. Pople, Self-Consistent Molecular Orbital Methods. XII. Further extensions of Gaussian-type basis sets for use in molecular-orbital studies of organic molecules, The Journal of Chemical Physics. 56, (1972), 2257. <https://doi.org/10.1063/1.1677527>
- [14] P. A. M. Dirac, Note on exchange phenomena in the Thomas atom, Mathematical Proceedings of the Cambridge Philosophical Society. 26, (1930), 376-385. <https://doi.org/10.1017/S0305004100016108>

- [15] J. P. Perdew, J. A. Chevary, S. H. Vosko, K. A. Jackson, M. A. Perderson, D. J. Singh, C. Fiolhais, *phys Rev, B* 46, (1992), 6671. <https://doi.org/10.1103/PhysRevB>.
- [16] D. M. Ceperley, B. J. Alder, Ground state of the electron gas by a stochastic method, *Physical Review Letters*. 45, (1980), 566-569. <https://doi.org/10.1103/PhysRevLett>.
- [17] A. D. Becke, Density-functional exchange-energy approximation with correct asymptotic behavior, *Physical Review A*. 38, (1988), 3098-3100. <https://doi.org/10.1103/PhysRevA>.
- [18] A. D. Becke, Density-functional thermo chemistry. II. The role of exact exchange, *The Journal of Chemical Physics* 98, (1993), 5648-5652. <https://doi.org/10.1063/1.464913>
- [19] P. Ghesquière, Rôle des glaces interstellaires dans la complexité moléculaire de l'espace: modélisation par les méthodes de la chimie théorique, Thèse de doctorat, (2015), Université de Montpellier.
- [20] C. A. Ullrich, *Time-Dependent Density-Functional Theory-Concepts and Applications*, Oxford University Press, New York, 44, (2012), pp. 286-288, 0103-9733
- [21] Y. R. Shen, *The Principles of Nonlinear Optics*, New York, Wiley, (1984), 576p. ISBN: 978-0-471-43080-3
- [22] M. Drissi, N. Benhalima, Y. Megrouss, R. Rahmani, A. Chouaih, F. Hamzaoui, Theoretical and experimental electrostatic potential around the m-nitrophenol molecule, *Molecules* 20, (2015), 4042–4054. <https://doi.org/10.3390/molecules20034042>
- [23] A. Djafri, Synthèse, étude structurale et propriétés physico-chimiques associées de quelques composés hétérocycliques, Thèse de doctorat en chimie, (2017), Université Abdelhamid Ibn Badis de Mostaganem.
- [24] C. C. J. Roothaan, New developments in molecular orbital theory, *Reviews of Modern Physics*, 23, (1951), 69-89. <https://doi.org/10.1103/RevModPhys.23.69>
- [25] R. J. Anderson, D. J. Bendell, P. W. Groundwater, *Organic Spectroscopic Analysis*, Royal Society of Chemistry, Cambridge, (2004). <https://doi.org/10.1021/np030773b>
- [26] T. M. Watson, J. D. Hirst, Density functional theory vibrational frequencies of amides and amide dimers. *The Journal of Physical Chemistry A*, 106, (2002), 7858-7867. <https://doi.org/10.1021/jp0255511>
- [27] G. Herzberg. Gerhard Herzberg and Bryce L. Crawford Jr. *Infrared and Raman spectra of polyatomic molecules*. D. Van Nostrand Company, 50 (3), (1945), 288-288, <https://doi.org/10.1021/j150447a021>
- [28] R. M. Silverstein, F. X. Webster, D. J. Kiemle, *Spectrometric identification of organic compounds*. John Wiley & Sons, (2014).

- [29] D. A. McQuarrie, J. D. Simon. Physical chemistry: a molecular approach. University Science Books, (1997).
- [30] R. R. Ernst, G. Bodenhausen, A. Wokaun, Principles of Nuclear Magnetic Resonance in one and two Dimensions. 2nd ed. Clarendon Press Oxford, 14, (1987), 640 p. ISBN: 0-19-855647-0
- [31] J. A. Tossell, Nuclear Magnetic Shieldings and Molecular Structure. 2nd ed. Springer Netherlands: Springer Science & Business Media, 386, (2012), 584p. <https://doi.org/10.1007/978-94-011-1652-7>
- [32] F. Jensen, Introduction to Computational Chemistry. United States: John Wiley & Sons, (2017).
- [33] H. Fukui, Methods of calculating NMR chemical shifts. Magnetic Resonance Review, 11, (1987).
- [34] G. Schreckenbach, T. Ziegler, The calculation of NMR shielding tensors based on density functional theory and the frozen-core approximation. International Journal of Quantum Chemistry, 60, (1996), 753-766. [https://doi.org/10.1002/\(SICI\)1097-461X](https://doi.org/10.1002/(SICI)1097-461X)

Chapter III:

Results and discussion

III.1. Introduction:

Spectroscopic methods provide a means to elucidate and validate the atomic arrangement within molecular structures, which may serve as fundamental components of intricate new organic molecular crystals. In theory, the spectroscopic assessment of each molecular structure is conducted after the molecular optimization, ensuring the absence of negative vibrational frequencies within the frequency calculation results for the $3N-6$ vibrational modes. This process affirms the optimized molecular configuration.

Consequently, our computational analysis of both compounds has been directed towards determining various molecular properties. This section will explore specific molecular characteristics delineating Complexes 1 and 2. The computational computations were primarily carried out using the Gaussian 09 software. In this chapter, specific physicochemical attributes are directly ascertained via Gaussian 09, while others have been computed with the supplementary computational software. Furthermore, the study of the anchor molecule of the two target compounds using the Autodock4.0 software.

III.2. The theoretical calculation methodology:

III.2.1. Calculation Details:

Theoretical calculations of quantum chemistry were made using the Gaussian program 09 [1]. Output files were visualized via Gauss View software 5 [2]. The structural properties of the Thione compounds were determined by applying the three-parameter hybrid functional Becke (B3) for the exchange part and function Lee-Yang-Parr correlation (LYP) [3] with the calculation base 6-311G(d,p) to obtain the optimized geometric parameters. The DFT method with the B3LYP and Gen are used to obtain the optimized molecular structure of complexes, in general, in the ground state and to calculate molecular parameters. The potential molecular electrostatic (MEP) and HOMO-LUMO energies were calculated at the same level. In addition, dipolar moment (μ), average polarizability (α), and first-order static hyperpolarizability (β) were all calculated in order to evaluate the non linear behavior of the compounds. The optimized structure of the thione molecules is shown on (Figure III.1.a, b).

III.2.2. Molecular geometries studied:

The molecular simulation for each investigated organic compound primarily relied on existing information regarding its basic molecular arrangement. This encompassed details such as the

chemical elements present, the atomic numbers of these elements, and the relative positioning of atoms with one another. This data was derived from the organic syntheses of these compounds [3].

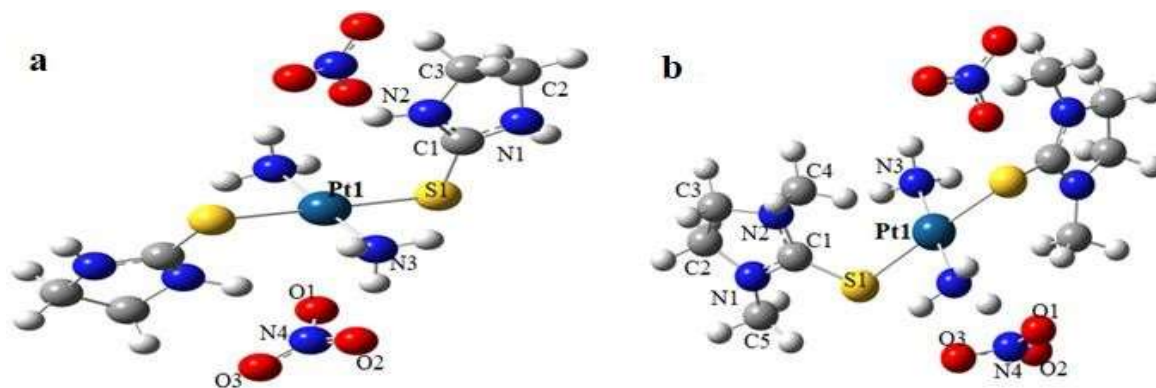


Figure III.1.a, b Optimization of complexes 1 and 2 ($\text{trans-}[\text{Pt}(\text{NH}_3)_2(\text{Imt})_2](\text{NO}_3)_2$ $\text{trans-}[\text{Pt}(\text{NH}_3)_2(\text{Me}_2\text{Imt})_2](\text{NO}_3)_2$).

III.3. Structure description:

In this part, we will examine specific geometric parameter values that define this molecular structure as determined experimentally and compared with those derived by molecular modeling. Details on the importance of interatomic distance angles of valence are given in (Table III.1).

The structures of the synthesized complexes (1–2) were optimized geometrically and shown in Figure III.1a,b. the bond distance, and bond angles of each compound were analyzed (Table III.4), specifically, atoms that are coordinated to the central metals such as nitrogen and sulfur (Table III.1).

The Pt metal atom is bonded to one N and one S atom with the respective bond distances; $\text{Pt1—N3} = 2.046\text{\AA}$, $\text{Pt1—S1} = 2.3260\text{\AA}$ for the $\text{trans-}[\text{Pt}(\text{NH}_3)_2(\text{Imt})_2](\text{NO}_3)_2$. The corresponding theoretical values are 2.0966\AA and 2.3971\AA estimated by the method DFT while $\text{Pt1—N3} = 2.054\text{\AA}$, $\text{Pt1—S1} = 2.3199\text{\AA}$ in $\text{trans-}[\text{Pt}(\text{NH}_3)_2(\text{Me}_2\text{Imt})_2](\text{NO}_3)_2$ are shown experimentally compared to the theoretical values of 2.088\AA and 2.394\AA , respectively. These measurements of bond distances closely match to the average values that have been reported for comparable complexes [4-5].

In a neutral environment, the central metal bands with the ligand via the sulfur atom, whereas in an essential domain, it forms bonds with both the sulfur and nitrogen atoms [6]. The Pt metal atom is bonded to two S and two N atoms. The N3i—Pt1—S1 bond angles around the

platinum are between 87.50° and 92.50° , as the trans angles in both are 180° , while in 2 the N3—Pt1—S1 angle is 88.52° and 91.48° for experimental and theoretical investigation respectively. The theoretical values show that the results are in good agreement with a high degree of accuracy and reliability in the DFT calculations, as they successfully capture the experimental structural features of the complexes.

Table III.1. Selected bond distances (\AA) and angles ($^\circ$) for 1 and 2.

Complex 1		
Bond Distance	Experimental	DFT
Pt1—N3	2.046	2,0966
Pt1—S1	2.3260	2,3971
Bond angles		
N3i—Pt1—N3	180	178,9
S1—Pt1—S1i	180	178,6
N3—Pt1—S1	92.50	89,7
N3i—Pt1—S1	87.50	88,7
Complex 2		
Bond Distance	Experimental	DFT
Pt1—N3	2.054	2,088
Pt1—S1	2.3199	2,394
Bond angles		
N3i—Pt1—N3	180	177,3
S1—Pt1—S1i	180	175,8
N3—Pt1—S1	88.52	88,9
N3i—Pt1—S1	91.48	93,05

III.4. IR analysis:

In comparison of these hybrid compounds, the theoretical and experimental infrared is shown in (Table III.2). It is widely recognized that infrared spectroscopy is a highly effective method for identifying functional groups within a molecular system [7], so it is a qualitative and quantitative analysis of many molecular species

In the table III.2 the C=S bond stretching vibrations of the aromatic ring for complexes (1) and (2) were calculated and located in the range of 1044–486 cm^{-1} , The same vibrations have been seen experimentally to be 1042–501 cm^{-1} for the first compound while it is ranged in 1058–483 cm^{-1} , and 1118–481 cm^{-1} for the calculated and the experimental results of the second compound, respectively.

The N–H stretching vibrations of the aromatic ring for both complexes were calculated and located in the 3476–1044 m^{-1} range comparable to those found experimentally to be 3310 and 1042 cm^{-1} in compound 1. As shown in (Table III.2), the calculated stretching vibrations of NO_3^- are expected to be around 836, 825, 839, and 827 cm^{-1} as experimental and theoretical values for complexes 1 and 2, respectively. A non-coordinated nitrate ion is credited with causing a distinct sharp band in both complexes, which is not observed in the free ligand [9]. Theoretically, the $\nu(\text{Pt-S})$ appeared in 283 cm^{-1} and 277 cm^{-1} theoretically which are close to the experimental values to be 272 and 265 cm^{-1} for complexes 1 and 2 respectively, agreeing the previous findings [10].

Table.III.2. Some influential IR Bands reveal the presence of the functional group characteristic of both complex forms.

Complex 1	Experimental	Theoretical
$\nu(\text{N-H})$	3310	3476
$\nu(\text{C=S})$	1042	1044
	501	486
$\nu(\text{NO}_3^-)$	836	839
$\nu(\text{Pt-S})$	272	283
Complex 2	Experimental	Theoretical
$\nu(\text{C=S})$	1118	1058
	481	483
$\nu(\text{NO}_3^-)$	825	827
$\nu(\text{Pt-S})$	265	277

III.5. Magnetic spectroscopic analysis:

Nuclear magnetic resonance (NMR) calculations were investigated using the gauge-independent atomic orbit (GIAO) approach through the employment of the DFT/6-311G (d, p) model [7]. The isotropic chemical shift values (d) for Tetramethylsilane (TMS) were calculated using the identical theoretical framework to compare the finding as a reference.

The ^1H and ^{13}C chemical shifts of the ligands and their platinum (II) complexes are listed in (Table III.3).

III.5.1. Magnetic spectroscopic analysis of complex 1:

The shifts listed in the table III.3 of these two compounds were computed relative to the shifts in the position of the carbon and hydrogen nuclei that correspond to the molecular structure of TMS. The experimental and theoretical findings regarding chemical shifts acquired through ^1H NMR and ^{13}C NMR analyses that define the molecular configuration of complex 1 are listed in (Table III.3).

- Proton nuclear magnetic resonance spectroscopy (^1H NMR):

The analysis of hydrogen nucleus shifts related to the molecular structure of complex 1 through position ^1H NMR spectroscopy reveals the presence of 9 protons within this structure. (Table III.3)

The computed ^1H NMR chemical shifts is 3,69 ppm for the H1, H2, H3, H4, H5, H7, H8, and H9 and vary from 1.14 to 5.35 for the experimental and theoretical values while the H6 show a remarkable discrepancy between theoretical and experimental calculation to be 13.01 and 9.09 ppm due to the use of solvent in the experimental study.

- Nuclear magnetic resonance spectroscopy of carbon (NMR ^{13}C):

The computed ^{13}C -NMR chemical shift values show a slight agreement between theoretical and experimental values.

III.5.2. Magnetic spectroscopic analysis of complex 2:

The study of Nuclear magnetic resonance shifts reveals to the presence of 13 protons and for carbons within this structure.

The computed ^1H -NMR chemical shifts, varies from 2.9279 to 7.7781ppm using the B3LYP/Gen / 6-311G (d, p) level, the experimental ones being in the range 3.65–3.65ppm, as it can be seen from the (Table III.3).

The calculated ^{13}C -NMR chemical shifts values is shown from 40.0491 to 197.293ppm. The experimentally measured values fall within the range of 50.29 to 166,89ppm.

Table III.3. Chemical displacements of complexes 1 and 2 obtained by ^1H NMR and ^{13}C NMR.

Complex 1			Complex 2		
^1H	Experimental	DFT	^1H	Experimental	DFT
H6	9,09	13.01	H1	3,65	7.77
H1	3,69	5.35	H2	3,65	3.41
H2	3,69	4.17	H3	3,65	2.92
H3	3,69	4.33	H4	3,65	4.12
H4	3,69	4.26	H5	3,65	3.88
H5	3,69	5.34	H6	3,65	3.92
H7	3,69	3.27	H7	3,65	4.07
H8	3,69	8.45	H8	3,65	4.89
H9	3,69	1.14	H9	3,29	3.27
^{13}C	Experimental	DFT	H10	3,29	3.38
C1	182,11	197.04	H11	3,29	4.51
C2	45.38	56.36	H12	3,29	6.65
C3	45,38	53.17	H13	3,29	0.55
			^{13}C	Experimental	DFT
			C1	166,89	197.29
			C2	50.29	57.12
			C4	50,29	40.04
			C5	36,07	42.68

III.6. Electronic structural properties:

III.6.1. Molecular Orbital Frontiers (FMO):

The frontier molecular orbitals known as HOMO and LUMO are essential in quantum chemistry while LUMO is the lowest unoccupied molecular orbital, and presents its capability to attract and capture an electron. Conversely, the HOMO, or highest occupied molecular orbital, is an energy level with occupied electrons, showing the ability to release an electron. These molecular orbitals play vital role in electron interactions within molecules. Measuring the energy difference between HOMO and LUMO, representing the energy gap, provides valuable insights into a molecule's chemical reactivity, optical polarizability, and chemical hardness [11].

A molecule with short gap exhibits higher polarizability and is typically linked to increased chemical reactivity and decreased kinetic stability [12]. Furthermore, the energy of the highest occupied molecular orbital (HOMO) is directly related to the ionization potential. In contrast, the energy of the lowest unoccupied molecular orbital (LUMO) is connected to the electron affinity. The interaction between these orbitals can lead to the occurrence of charge transfer [7].

HOMO energy is -6.0274 eV, and LUMO level energy is -2.0621 eV for the first compound to present an energy gap of 3.9680 eV. Thus, the energy values for the HOMO⁻¹, and LUMO⁺¹ are -6.0292, and -1.1445 eV, respectively. The disparity in energy between these two orbitals is 4.8829 eV. The positive phase is in red while the negative phase is green colored, which means the red phase is the acceptor phase, and the green phase is the donor portion [8]. These molecular orbitals of compound 1 are shown in (Figure III.2) where the molecular orbitals of compound 2 are HOMO = -5.4303 eV, LUMO = -2.1666 eV, and the energy gap is 3.2637 eV.

The interaction between these orbitals leads charge transfer. As it is shown the HOMO-1 is concentrated on thione ring and in nitro group and central metal. The HOMO is denser on nitro group. This observation was also remarkable in the second complex. as illustrated in (Figure III.2). Within the engaged molecular orbitals, the Highest Occupied Molecular Orbital (HOMO) and the HOMO-1 are predominantly concentrated around the C-S bond due to the lone pair of electrons in the sulfur atom [13]. Conversely, within the unoccupied molecular orbitals, the Lowest Unoccupied Molecular Orbital (LUMO) and LUMO+1 display dispersion across the other parts of the molecular fragments. This dispersion could facilitate intramolecular charge transfer during transitions between states.

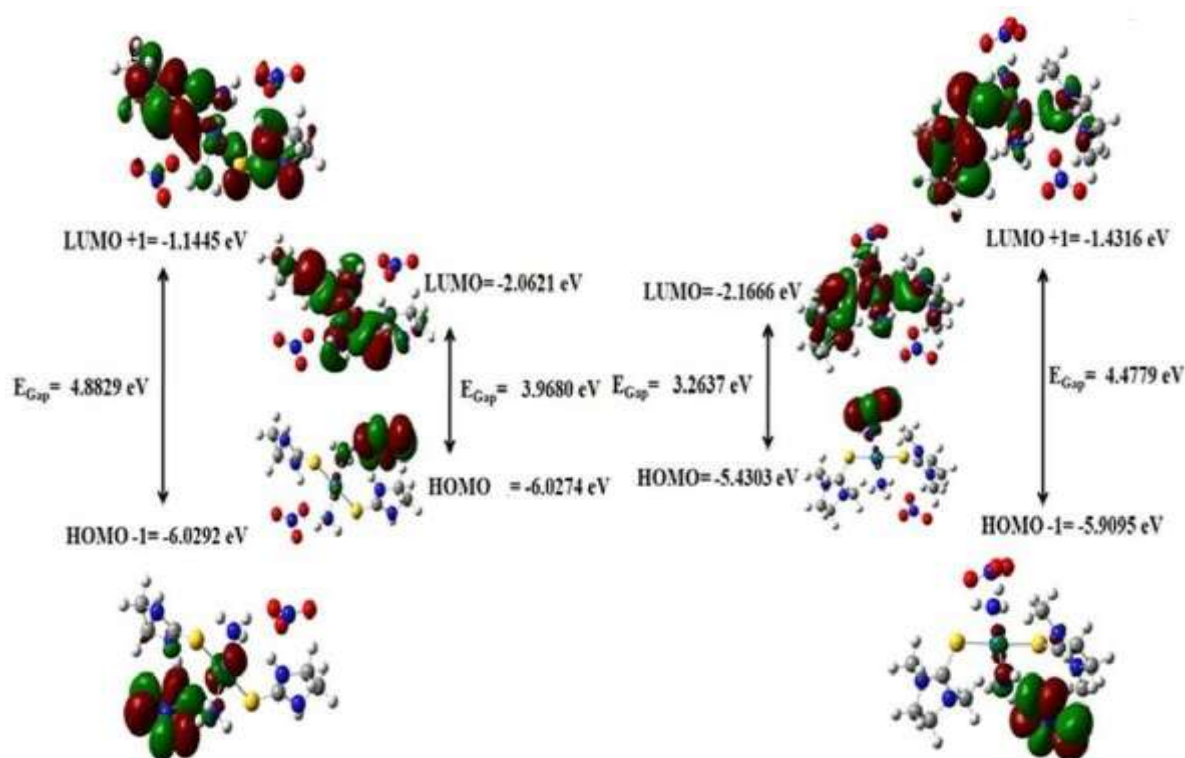


Figure III.2.Representation of Molecular Orbital Frontiers of compound 1 and compound 2.

Global chemical Reactivity Descriptors:

Following existing literature, chemical hardness and softness represent two parameters influencing the stability of organic compounds which are known as Global Chemical Reactivity Descriptors GCRD. These GCRD parameters elucidate the electronic interactions among molecular constituents [15].

The variations of GCRD elucidate the electronic interactions among molecular orbitals utilizing the ionization potential ($I.P. = -E_{HOMO}$) and the electron affinity ($E.A. = -E_{LUMO}$), the GCRD characteristics, encompassing attributes such as electronegativity (χ), chemical potential (μ), chemical hardness (η), chemical softness (s), as well as electrophilicity (ω) and nucleophilicity (ϵ) indices, that can be derived using the subsequent equation:

$$\chi = \frac{(IP + EA)}{2}; \mu = -\frac{(IP + EA)}{2}; \eta = \frac{(IP - EA)}{2}; S = \frac{1}{2\eta}; \omega = \frac{\mu^2}{2\eta}; \epsilon = \frac{1}{\omega} \quad (\text{eqIII.1})$$

According to (Table III.4), the calculated values of the GCRD parameters are $\eta = 1.9826$ eV for complex 1 and $\eta = 1.8714$ eV for complex 2. The structure stability of

the title compound is confirmed by the negative value of the chemical potential [7] $P = -4,0447\text{eV}$ for complex 1

and $P = -4.0380\text{eV}$. This stability is also guaranteed by the positive value of the hyperhardness index η , which indicates that the charge transfer within the molecule is favorable. The calculated values of GCRD parameters for complex 1 and complex 2 are summarized in (Table III.4).

Both complexes have the lowest energy gap, revealing that the molecule is kinetically stable. This stability is also confirmed by the positive value of the hyperhardness index (Table III.4). The chemical hardness (1.9826 eV) for complex 1 and (1.8714eV) for complex 2 indicate that charge transfer occurs within the molecule. Furthermore, the molecule's electrophilicity is confirmed by the global electrophilicity, which has a value of 4.1256 eV for complex 1 and 4.3564 for complex 2.

The complex with the most significant energy gap among these two compounds is complex 1 (Table III.4). As a result, it stands as the more stable molecule and exhibits lower reactivity.

Table III.4. GCRD calculated values for complexes 1 and 2 by B3LYP/6–311G(d,p).

Parameters	Calculated energies (eV) for Complex 1	Calculated energies (eV) for Complex 2
E_{HOMO}	-6.0274	-5.9095
E_{LUMO}	-2.0621	-2.1666
$E_{\text{HOMO}-1}$	-6.0292	-5.4303
$E_{\text{LUMO}+1}$	-1.1445	-1.4316
Energie gap (ΔE)	3.968	3.2637
Ionization potential (I)	6.0274	5.9095
Electron affinity (A)	2.0621	2.1666
Electronegativity (χ)	4.0447	4.0380
Chemical potential (P)	-4.0447	-4.0380
Chemical hardness (η)	1.9826	1.8714
Chemical softness (s)	0,2521	0.2671
Electrophilicity index (ω)	4.1256	4.3564
Nucleophilicity index (ε) (eV^{-1})	0.2423	0.2295

III.6.2. Molecular electrostatic potential analysis:

Understanding molecular interactions requires studying the molecular electrostatic potentials (MEPs). The color variation on a surface reveals a molecule's dimensions and form, along with individual atoms electrostatic potential values. This helps predict molecular arrangement and physicochemical properties. Gaussian 09 software was used to determine charge distribution on organic systems' molecular surfaces, predicting favorable hydrogen-type interaction sites [7].

The color transition observed in (Figure III.3), progressing from blue to red, illustrates distinct electrostatic potential levels that follow the sequence red < orange < yellow < green < blue [14]. Within this sequence, blue signifies the highest positive charge, while red indicates a predominantly negative charge. Negative potential zones denote locations conducive to protonation or nucleophilic interactions, whereas positive potential areas are associated with electrophilic interactions. In this map drawing, the zones around the NO₃ group are depicted in red, meaning these regions are rich in electrons. For the most favorable region of both complexes, (Figure III.3) shows that the region around the hydrogen atoms is the electron-poor region, whose aromatic protons have small positive charges and are represented by a light blue color.

The electrostatic potential values of the molecular structures for compound 1 and compound 2 were depicted using color gradients between two contrasting values. Compound 1's lower limit was set at $-7.107e-2$, while the upper limit was at $7.107e-2$. As for compound 2 the lower limit was $-8.434e-2$, and the upper limit was $8.434e-2$. A visual representation of the Molecular Electrostatic Potential (MEP) graph for both structures is shown in (Figure III.3).

Analysis of the Complex 1 electrostatic potential map shows that:

- The molecular regions with negative polarization are depicted in shades of red and yellow. These hues were positioned around the oxygen atom O1 and the sulfur atom S1. These regions are notable for having the lowest electrostatic potential values, indicating a higher electronic density. Consequently, these areas represent electrophilic sites.
- The molecular regions exhibiting positive polarization are depicted in blue. These regions are on hydrogen atoms associated with thione rings and methyl groups. They are distinguished by the highest electrostatic potential values, indicating a lower electron density. Consequently, these areas function as nucleophilic sites.
- Within the examined molecular structure, regions that approached neutrality were represented as green.

Regarding the molecular configuration of complex 2, the electrostatic potential map was illustrated using molecular potential values bounded by two distinct limits as specified (Figure III.3).

In a ribbon format, reactive sites are delineated by colors representing electron density or electrostatic potential across the molecule's electrophilic, nucleophilic, and neutral regions. Red signifies the most electronegative zone where the electron density reaches its maximum. This is mainly associated with the nitrogen atoms of NO₃, which are also involved in hydrogen bonding, both of which function as electron acceptors in the structure. Hence, they are prone to nucleophilic attacks (electrophilic regions).

Conversely, the most electropositive areas, characterized by minimal electron density, are depicted in blue, corresponding to the methylene group of the thione cycle. This site is favorable for nucleophilic attacks (nucleophilic regions).

The observed surface pattern indicates that the studied molecular geometry has the potential to engage in molecular interactions at both the carbonyl and imine groups (acting as electron acceptors), as well as the methylene group of the thione cycle (functioning as electron donors). This observation aligns well with the presence of hydrogen bonds that connect molecules within the crystal structure of compound 2.

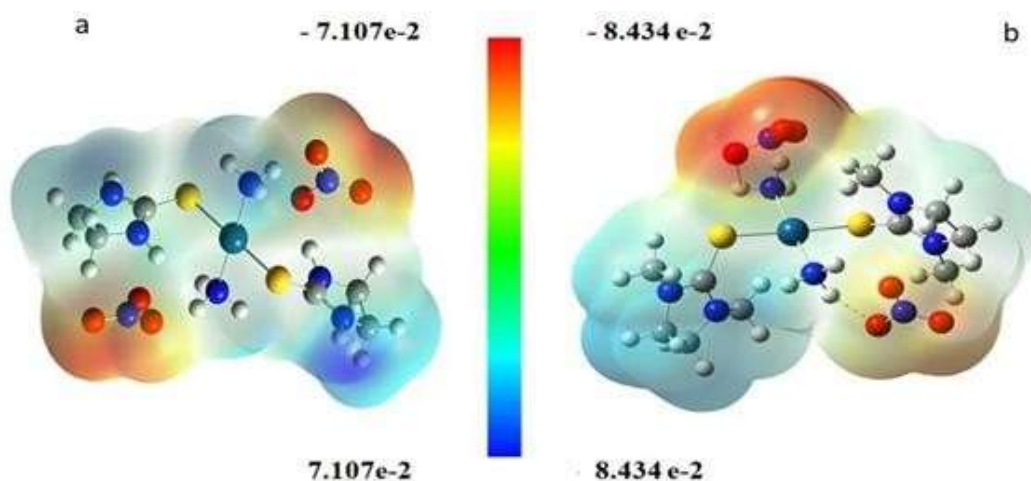


Figure III.3. Molecular electrostatic potential of complex 1 and complex 2.

Hirshfeld surface analysis:

The Hirshfeld surface (H.S.) analysis is crucial for investigating molecule interactions [7]. We can explore the molecular interactions in the crystalline environment using H.S. outputs. The

following equation describes the d_{norm} (normalized connection distance), which is calculated from the atoms' d_e , d_i , and van der Waals radii (r_i^{vdw} and r_e^{vdw}):

$$d_{norm} = \frac{d_i - r_i^{vdw}}{r_i^{vdw}} + \frac{d_e - r_e^{vdw}}{r_e^{vdw}} \quad (\text{eq III.2})$$

In this context, d_e and d_i represent the nearest distances from the location to the closest nucleus, where d_e pertains to internal space, and d_i pertains to external length. The three-dimensional Hirshfeld surface (3D-HS) visualization and the corresponding two-dimensional fingerprint diagrams were generated using the CrystalExplorer21 software [16].

This H.S. has three colors (red, white, and blue). The short and long contacts are symbolized by the red and blue dots, respectively. White spots or areas on the H.S. depict connections where the distance between atoms is the same as the combined van der Waals radii [15].

The Hirshfeld surfaces of complexes 1 and 2 mapped over d_{norm} proved to be very similar (Figure III.4). The red spots indicating strong interactions are found at both hydrogen atoms of the N.H. fragments and in the area of the nitrogen lone pair of the amino group. In addition, red spots are seen at the sulfur atom [17].

The significant deep-red spots on the density-normalized heat map suggest that the interactions nearby, primarily responsible for forming hydrogen bonds, are being highlighted.

(Figure III.5.A) illustrates the 2D fingerprint plot, showcasing the essential surface contacts crucial for organic molecules, which are the H-H contacts with a contribution of (31.2%) to the H.S. of the title molecule. O-H/H-O (49.3) contact regions occupy the remaining area of the fingerprint plot, and the most important contributions to the H.S. are S-H/HS (8.3%), H-N/N-H (3.5%) and S-S (1.9%).

The two-dimensional (2D) fingerprint plot is illustrated in (Figure III.5.B) using d_e and d_i distances. As shown in the figure, the H-H interactions contribute with an overall H.S. of 42.2% and appear in the center of the scattered points. Except for H-H interactions, representing the majority of contacts of the title molecule, the most important contributions to the H.S. come from H-C/C-H (2.2%) and S-H/H-S (5.8%) contacts. Other intermolecular interactions contributing to H.S. are H-O/O-H (40.9) and H-O/O-H (40.9) contact regions.

Analysis of the fingerprint plots showed strong intermolecular interactions indicated as sharp spikes (Figure III.5.A,5.B). H.H. interactions in both molecules significantly contribute to the total Hirshfeld surface (Figure III.5.A,5.B). The contributions of SH/HS and CH/HC interactions associated with X—H.S. and X—H.C. hydrogen bonds are similar. Surprisingly, the contribution of NH/HN interactions proved to be the lowest (Figure III.5.A). It may be

explained by the participation of the nitrogen lone pair in hydrogen bonding as a proton acceptor.

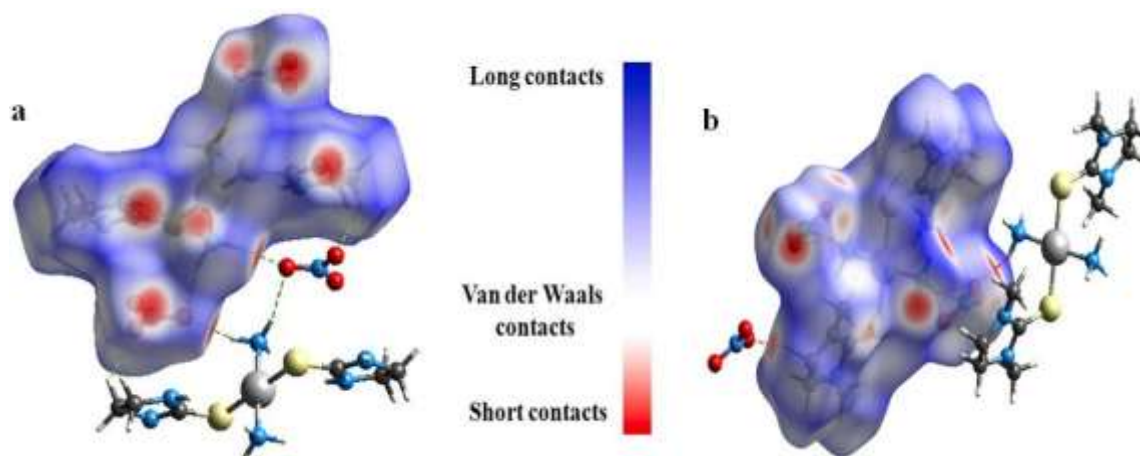


Figure III.4. Hirshfeld surfaces for visualizing with d_{norm} selected the intermolecular contacts of the complexes 1 and 2.

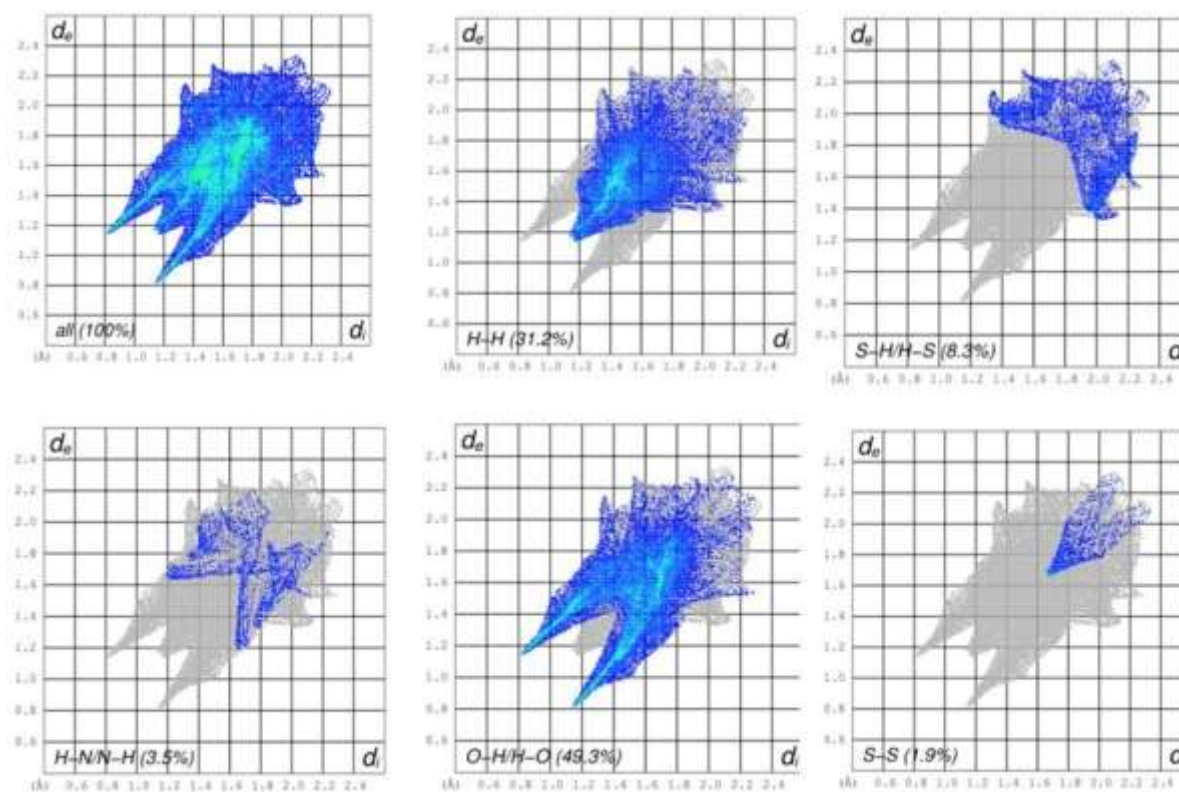


Figure III.5. A. Two-dimensional fingerprint plots of complex 1 with d_{norm} selected intermolecular contacts.

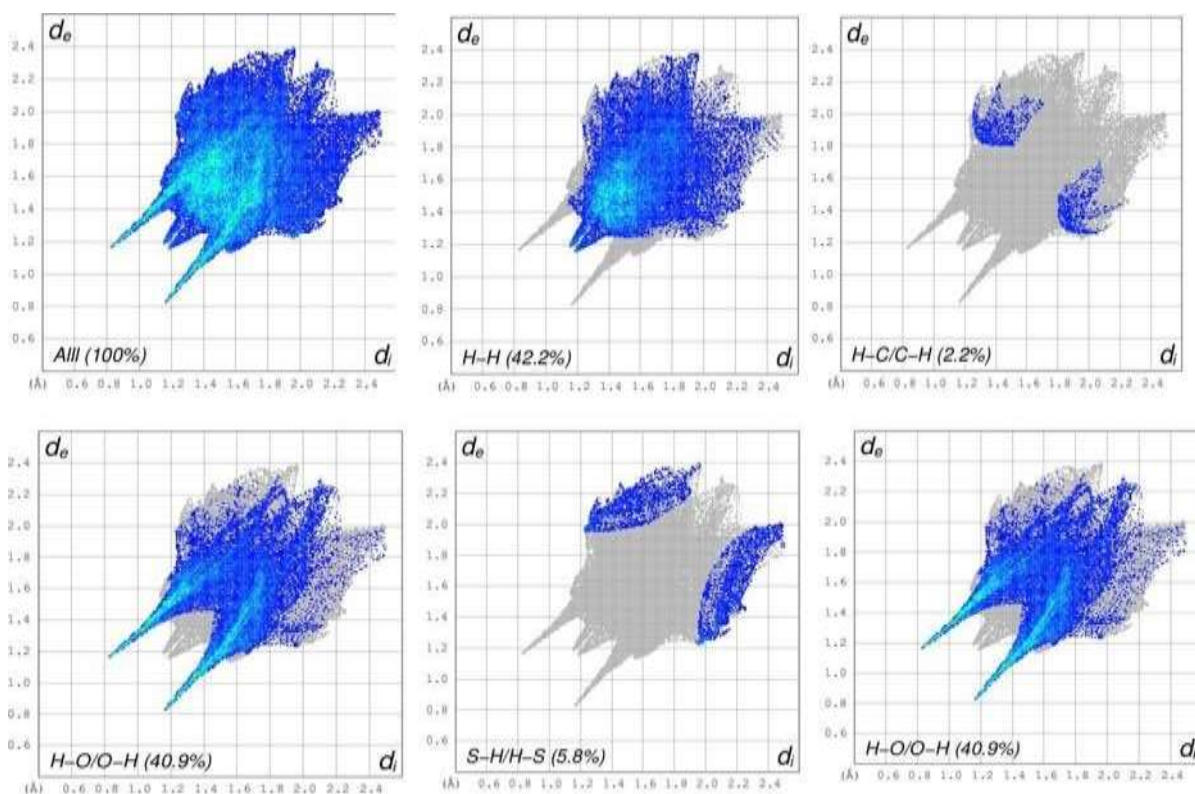


Figure III. 5. B. Two-dimensional fingerprint plots of complex 2 with d_{norm} selected intermolecular contacts.

Figure III.5. Two dimensional fingerprint plots of the complexes 1 and 2 with d_{norm} selected intermolecular contacts.

Nonlinear optical properties:

Electromagnetic interactions within different mediums give rise to novel fields exhibiting unique stages, ultimately resulting in the nonlinear optical (NLO) phenomenon. This effect holds significant potential for emerging technologies such as telecommunications and signal processing, offering diverse capabilities [7].

The calculated results have been converted into electrostatic units (esu) (α : 1 a.u. = 0.1482×10^{-24} esu, β : 1 a.u. = 8.6393×10^{-33} esu and for γ : 1 a.u. = 5.03670×10^{-40} esu).

The listed values for complex 1 and complex 2 in Table 3 include the computed dipole moment (μ), isotropic polarizability (α), first-order hyperpolarizability (β), and dynamic second-order hyperpolarizability (γ). The values of the dipole moment of complex 1 and complex 2 are obtained respectively from B3LYP functional are equal to 3.17538 and 11.6018 D, The values closely resemble those found in existing literature for organic compounds [18]. The most incredible dipole moment value is observed for the μ_z component [9]. Furthermore, The polarizability static is found to be 35.0713×10^{-24} and 42.7482×10^{-24} respectively for both

complexes. Regarding this parameter, the α_{xx} component exhibits the highest value, measuring 307.690 (au) for complex 1 and 370.967 (au) for complex 2. This indicates a significant extent of delocalization along this direction [19]. Compared to complexes 1 and 2, the B3LYP/6-311G functional gives a better value of the dipole moment, which means the second complex has a better value of the dipole moment. In light of these findings, both complexes could be classified as typical molecules for NLO applications [7] (Table III.5).

Table III.5. Calculated molecular dipole moment (μ), polarizability (α), and first and second hyperpolarizabilities (β and γ) values for complexes 1 and 2.

Dipole Moment	Complex 1	Complex 2
μ_x	3.17538	-8.16902
μ_y	0.000000	-7.18524
μ_z	0.000000	-4.03005
$\mu(\text{Debye})$	3.17538	11.6018
Polarizability	$\alpha(0;0)$	
	Complex 1	Complex 2
α_{xx}	307.690	370.967
α_{yx}	18.9465	15.2379
α_{yy}	186.269	256.283
α_{zx}	52.9184	-14.3228
α_{zy}	18.0692	17.8912
α_{zz}	216.058	238.188
$\alpha(\text{au})$	236.673	288.479
$\alpha(\times 10^{-24} \text{ esu})$	35.0713	42.7482
First-order hyperpolarizability	$\beta(0;0,0)$	
	Complex 1	Complex 2
β_{xxx}	249.888	-304.14
β_{xxy}	81.6154	-49.4839
β_{yyx}	85.3502	-357.903
β_{yyy}	85.6534	-384.207
β_{xxz}	37.5180	-18.816
β_{yxz}	21.3832	-27.3804
β_{yyz}	56.7751	-79.1001
β_{zxx}	46.9293	72.0277
β_{zyz}	61.0746	-26.298
β_{zzz}	59.4819	-305.637
$\beta(\text{au})$	92.2650	504.3
$\beta(\times 10^{-30} \text{ esu})$	0.797097	4.35676
Second-order hyperpolarizability	$\gamma(0;0,0,0)$	
	Complex 1	Complex 2
γ_{xxxx}	93459.3	33.1739
γ_{xxyy}	16064.8	6.66704
γ_{yyyy}	31493.5	21.7338
γ_{xxzz}	20439.7	17.5859
γ_{yyzz}	7545.92	9.13866
γ_{zzzz}	31002.6	48.6406
$\gamma(\text{au})$	48811.9	67636.2
$\gamma(\times 10^{-36} \text{ esu})$	24.5851	34.0663

III.7. Biological activity:

III.7.1. Introduction:

With 2 million cases expected in 2020 [20], lung cancer is one of the most common cancer types in the world. Similar incidence and mortality statistics apply to liver cancer, with low- and middle-income nations accounting for 70% of all cancer-related deaths [21]. Normal cells don't divide unless they get a chemical signal from the nucleus, and when DNA is harmed, it either instructs the cell to repair itself or to program cell death. Cancer cells proliferate randomly and divide uncontrollably as a result of DNA aberration, accumulating cells that eventually form a tumour mass. Malignant tumours can invade nearby organs, intravasate into blood arteries, and spread to other bodily regions, creating new secondary tumours known as metastases, which can be fatal [22]. Some tumours have weak invasive capacity and do not move into other tissues. About 90% of cancer-related deaths are linked to metastasis, which highlights the inability to control the condition once it has spread throughout the body. All malignancies are thought to result from alterations in DNA sequences, which modify important genes and alter the activity of affected cells. When cells replicate, mutations can happen naturally or as a result of external factors such poor nutrition, tobacco use, infections, obesity, alcohol use, and exposure to UV radiation, pollution, and certain chemicals [23].

III.7.2. Cell lines:

Cell lines are a valuable tool in scientific research due to their cost-effectiveness, ease of use, unlimited material supply, and ethical concerns. They have revolutionized vaccine production, drug metabolism, antibody production, gene function study, artificial tissue generation, and biological compound synthesis [24]. However, cell lines must maintain functional features close to primary cells, as their functions are often not fully understood. Genetic manipulation can alter their phenotype, native functions, and responsiveness to stimuli. Serial passage of cell lines can cause genotypic and phenotypic variation over time, and genetic drift can cause heterogeneity in cultures. Cell lines may not adequately represent primary cells and may provide different results [25]. Major problems associated with cell lines include contamination with other cell lines and mycoplasma. Cross-contamination of cell lines, either inter or intraspecies, has been exposed since the early 1970s. Therefore, great care should be taken

when using cell lines and experiments with key findings confirmed in primary cultures should always be included.

Chemotherapy, a method of using chemical substances to treat or induce disease changes, has been widely used since the early 20th century. Metal compounds like antimony, bismuth, gold, iron, silver, and platinum are used for their antitumor properties. Cisplatin (VI) complexes, specifically cis-5 diamminedichlorid-platinum(II) (Cisplatin), is a pivotal development in creating novel cancer treatment agents (Figure III.6).



Figure III.6.Structure of Cisplatin.

Cisplatin's cytotoxicity arises from its ability to form covalent crosslinks with DNA, causing distortion in the helical structure and consequently inhibiting DNA replication and transcription [26]. Specifically, platinum ions covalently bond to deoxyribonucleic acid (DNA), particularly at the N7 position of guanine or adenine within the nucleotide sequences GAG and ACG, forming inter-strand crosslinks [27]. This cisplatin-DNA complex activates a novel cellular pathway that inhibits transcription, halting the cell cycle, impeding DNA repair, and ultimately triggering apoptosis[28], as shown in (Figure III.7).

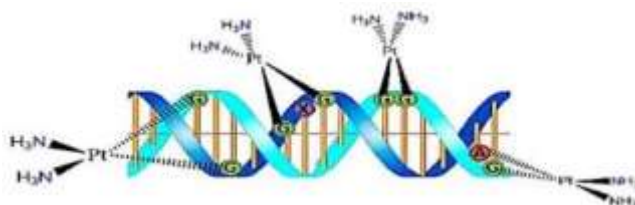


Figure III.7.Binding of cisplatin moiety with deoxyribonucleic acid in DNA.

Cisplatin and carboplatin are well-established anticancer medications used in global chemotherapy, benefiting hundreds of thousands of cancer patients. However, concerns include resistance and potential neuro-toxic side effects. Platinum-based drugs primarily target DNA, but they also interact with sulfur-containing biomolecules, particularly thiones. New metal complexes with S-donor atom ligands have shown promising cytotoxic and anticancer activities. Many platinum-containing complexes, such as heterocyclic and aliphatic thiones, have shown cytotoxic and anticancer activities, sometimes higher than cisplatin. These complexes are considered potential anticancer agents.

Molecular docking analysis:

Computer-aided drug design faces challenges due to its lack of clear engineering design rules and the complexity of biological processes involved in drug actions and metabolism at the molecular level. Despite this, molecular modeling, computer-aided drug design methods, data analysis, and chemo-informatics approaches have become crucial tools for drug discovery and have been successfully applied to medicinal chemistry.

Protein Data Bank (www.rcsb.org/pdb) was used to locate the four distinct 3D crystal structures of the cyclin-dependent kinase CDK6 protein (PDB IDs 4EZ5). This updated PDB files were then converted to PDBQT using MGLtools 1.5.6 specifying the active site. For 4EZ5, a grid box of 60, 36, and 32 points in the x, y, and z directions was constructed and centred on the ligands (the complex 1 and 2) with a spacing of Cartesian coordinates were -3.889, 7.472, and -8.278 in x, y, and z, respectively. The *gpf* and *dpf* files were updated to include metal ion parameters for use in the docking computation. Using PyMOL, a molecular graphics program, and AutoDock Tools 1.5.6, the docked stance has been visualized [29].

The (Table III.6) and (Table III.7) displays the docking binding energies of the studied Pt complexes 1 and 2 with the targets which were -5.19 and -6.40 kcal/mol, respectively while the lowest binding energies for docking (kcal/mol) in the *dlg* output file in Autodock were regarded as answer after every run. As listed in (Table III.6,7) for the complexes 1 and 2, respectively.

The intermolecular interactions (Table III.8) between the ligand 1/4EZ5 and the ligand 2/4EZ5 are shown in (Figures III.8 to III.9). For the 4EZ5 protein, the docking results show six strong conventional hydrogen bonds. These intermolecular interactions are observed between the O2 atom of the NO3 group and GLY411, SER413, GLN409, ARG414, ARG414, and ASP377 residues with distances of 2.752382, 2.145949, 2.172381, 2.471731, 2.081133, and 2.225128 Å, respectively. While, one Conventional Hydrogen Bond and four Carbon Hydrogen Bond were observed between MET431, ASN448, SER446, and MET452 residues and NH3 and Me2Imt groups. The above cited interactions are shown in (Figure III.8) and (Figure III.9) These results show a good satisfactory with literature results [30]. The docking results indicate that the ligands possess antitumour activity, suggesting that the compounds may be strongly recognized as a suitable inhibitor of the cyclin-dependent kinase CDK6 protein.

Table III.6. Binding affinity and RMSD values of different poses in the 4EZ5 inhibitor of by Auto Dock 4.

Sub-Rank	Binding Energy (kcal/mol)	Cluster RMSD	Reference RMSD
1	-5.19	0.00	126.80
2	-5.14	0.08	126.79
3	-5.13	0.10	126.81
4	-5.04	0.12	126.80
5	-5.03	0.47	126.60
6	-4.92	0.24	126.74
7	-4.62	1.02	127.08
8	-4.53	0.64	126.80
9	-4.47	1.19	127.10
10	-4.45	1.03	127.10

Table III.7. Binding affinity and RMSD values of different poses in the 4EZ5 inhibitor of by Auto Dock 4.

Sub-Rank	Binding Energy (kcal/mol)	Cluster RMSD	Reference RMSD
2	-6.40	0.36	113.15
3	-6.25	0.61	113.43
4	-6.21	1.73	112.31
5	-6.18	0.46	113.14
6	-6.16	1.79	113.89
7	-6.06	1.47	112.79
1	-6.27	0.00	113.48
1	-6.12	0.00	111.92
2	-6.10	0.75	112.01

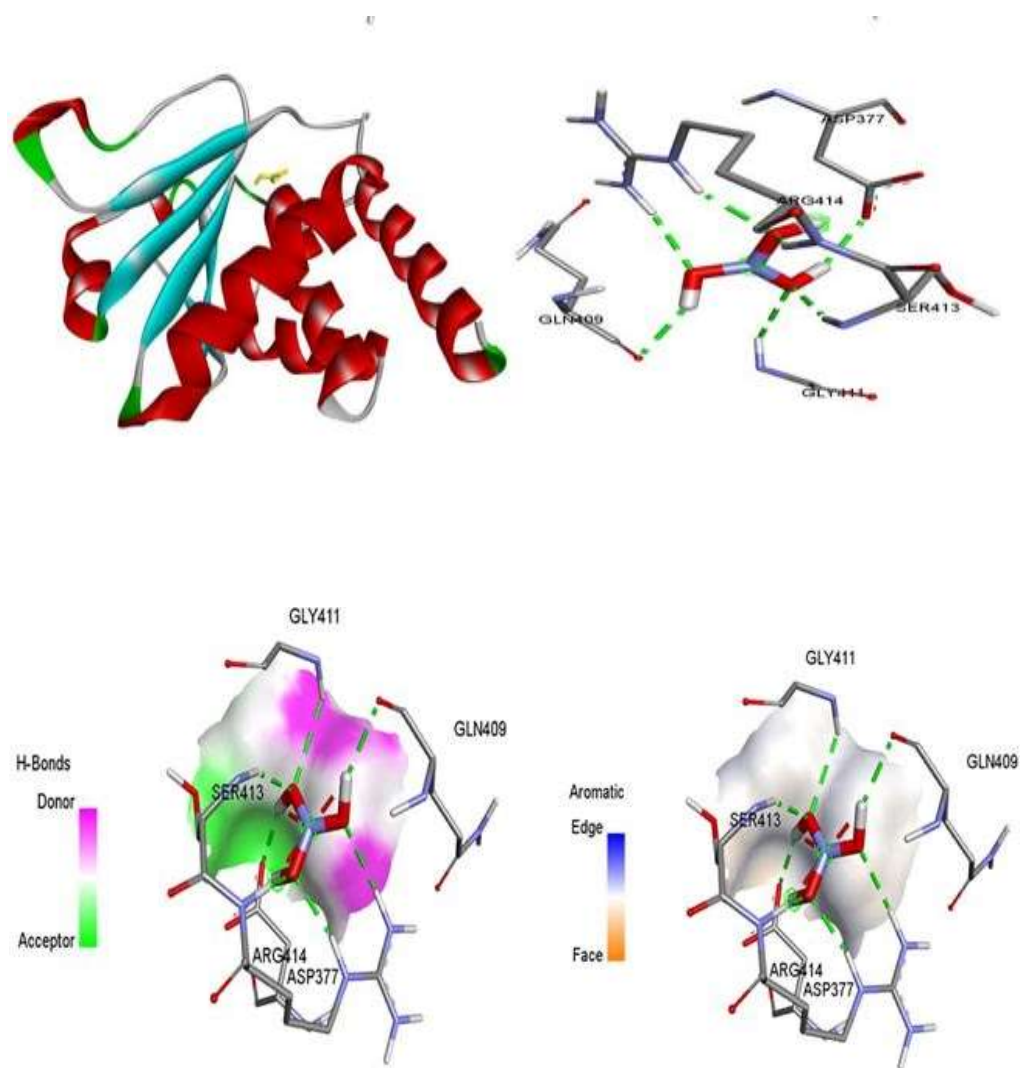


Figure III.8. (a) 3D ribbon structure of receptor/4EZ5 protein, (b) interaction between the active site residues of the protein and Complex 1.

Table III.8. Distance types and location of intermolecular interactions formed from the residues of the protein cyclin-dependent kinase CDK6 (PDB ID: 4EZ5) and the complex 1 and 2.

Protein Ligand	Residue	Moiety	Category	Types	Distance (Å)	
PDB ID: 4EZ5	Complex 1	A:GLY411	Oxygen	Hydrogen Bond	Conventional Hydrogen Bond	2,752382
		A:SER413	Oxygen	Hydrogen Bond	Conventional Hydrogen Bond	2,145949
		A:GLN409	Oxygen	Hydrogen Bond	Conventional Hydrogen Bond	2,172381
		A:ARG414	Oxygen	Hydrogen Bond	Conventional Hydrogen Bond	2,471731
		A:ARG414	Oxygen	Hydrogen Bond	Conventional Hydrogen Bond	2,081133
		A:ASP377	Oxygen	Hydrogen Bond	Conventional Hydrogen Bond	2,225128
PDB ID: 4EZ5	Complex 2	A:MET431	NH3	Hydrogen Bond	Conventional Hydrogen Bond	2,240296
		A:ASN448	Me2Imt 1i	Hydrogen Bond	Carbon Hydrogen Bond	3,396737
		A:SER446	Me2Imt 1i	Hydrogen Bond	Carbon Hydrogen Bond	3,599885
		A:MET452	Me2Imt 1	Hydrogen Bond	Carbon Hydrogen Bond	3,305296
		A:MET452	Me2Imt 1	Hydrogen Bond	Carbon Hydrogen Bond	3,142893

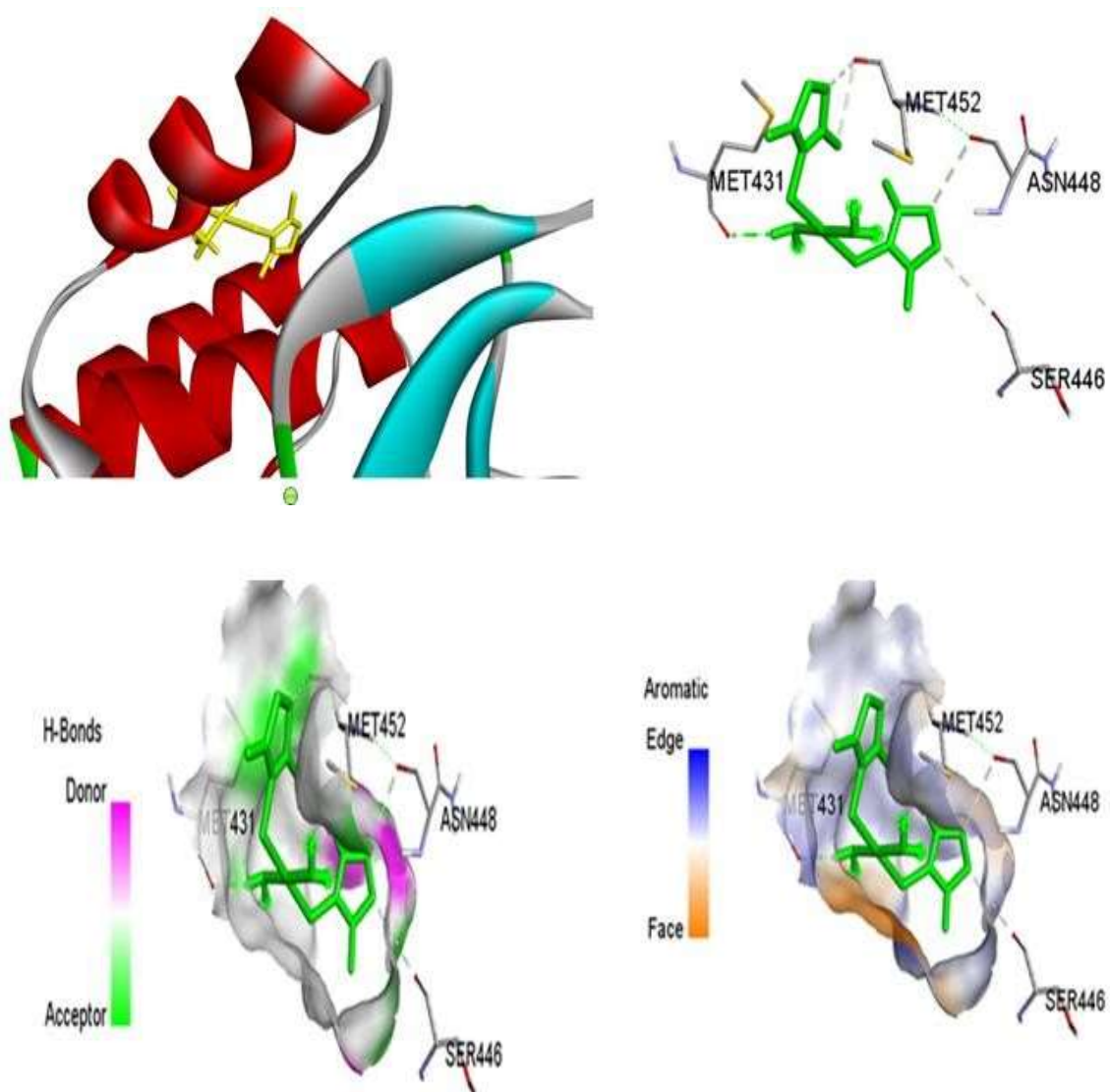


Figure III.9. (a) 3D ribbon structure of receptor/4EZ5 protein, (b) interaction between the active site residues of the protein and Complex2.

III.8. Conclusion:

Results of theoretically spectroscopic analysis of the trans-[Pt(NH₃)₂(Imt)₂](NO₃)₂ and the trans-[Pt(NH₃)₂(Me₂Imt)₂](NO₃)₂ showed a good correlation with those predicted experimentally. Some discrepancy was noted between the values observed in the experimental and the calculated NMR mainly due to the effect of the solvent (DMSO) used. In addition, in infrared spectroscopy, Owing to the absence of anharmonic contributions in the theoretical calculations, a slight difference was remarkable in the frequencies. The analysis of the electronic and optoelectronic properties of the two organometallic compounds reveals to predict the relationship between structure properties of molecular system. The overall electronic behavior of each compound was evidenced by the reorganization energy of electrons as well as the global reactivity indices based on the frontier molecular orbitals HOMO and LUMO. The results obtained from the calculation of the dipole moment, static polarizability and the first-order hyperpolarizability using the functional B3LYP based on 6-311G (d, p) and Gen basis sets for organic atoms and the metal, respectively; give a more favourable value to promote the trans-[Pt(NH₃)₂(Imt)₂](NO₃)₂ as a good candidate for optoelectronic field. Finally, the molecular docking study of the compounds inhibitory effect against the protein cyclin-dependent kinase CDK6 with the PDB ID: 4EZ5 was investigated using autodock4 software. This study shows a binding energy of -5.19 and -6.40 kcal/mol for the complexes 1 and 2, respectively; and explores the inhibitory effect against the protein cyclin-dependent kinase CDK6 derived from the A549 cell.

Bibliographical references:

- [1] M. J. Frisch, G. W. Trucks, H. B. Schlegel, G. E. Scuseria, M. A. Robb, J. R. Cheeseman, G. Scalmani, V. Barone, B. Mennucci, G. A. Petersson, H. Nakatsuji, M. Caricato, X. Li, H.P. Hratchian, A. F. Izmaylov, J. Bloino, G. Zheng, J. L. Sonnenberg, M. Hada, M. Ehara, K. Toyota, R. Fukuda, J. Hasegawa, M. Ishida, T. Nakajima, Y. Honda, O. Kitao, H. Nakai, T. Vreven, J. A. Montgomery, Jr., J. E. Peralta, F. Ogliaro, M. Bearpark, J. J. Heyd, E. Brothers, K. N. Kudin, V. N. Staroverov, R. Kobayashi, J. Normand, K. Raghavachari, A. Rendell, J. C. Burant, S. S. Iyengar, J. Tomasi, M. Cossi, N. Rega, J. M. Millam, M. Klene, J. E. Knox, J. B. Cross, V. Bakken, C. Adamo, J. Jaramillo, R. Gomperts, R. E. Stratmann, O. Yazyev, A. J. Austin, R. Cammi, C. Pomelli, J. W. Ochterski, R. L. Martin, K. Morokuma, V. G. Zakrzewski, G. A. Voth, P. Salvador, J. J. Dannenberg, S. Dapprich, A. D. Daniels, Ö. Farkas, J. B. Foresman, J. V. Ortiz, J. Cioslowski, D. J. Fox, Gaussian 09, Revision D.01 (Computer Software), Gaussian, Inc., Wallingford, CT, United States, (2013).
- [2] R. Dennington, T. Keith, J. Millam, GaussView Version 4.1.2, Semichem Inc., Shawnee Mission, K. S, (2007).
- [3] N. E. H. Belkafouf, Thèse de Doctorat Analyse structurale et spectroscopique de nouveaux matériaux fonctionnels, (2019), Université Abdelhamid Ibn Badis de Mostaganem.
- [4] S. Ahmad, R. Seerat-ur, T. Rüffer, T. Khalid, A. A. Isab, A. R. Al-Arfaj, M. Saleem, Ejaz, I. U. Khan, M. A. Choudhary, Synthesis, x-ray structures and cytotoxic behavior of platinum (II) complexes of dithiocarbamates, *Monatsch. Chem*, 148, (2017), 669-674. 1328267
- [5] A. Z. A. Mustafa, M. Altaf, M. Monim-ul-Mehboob, M. Fettouhi, M. I. M. Wazeer, A. A. Isab, V. Dhuna, G. Bhatia, K. Dhuna, Tetrakis(1-3-diazinane-2-thione)platinum(II) chloride monohydrate complex: Synthesis, spectroscopic characterization, crystal structure and in vitro cytotoxic activity against A549, MCF7, HCT15 and HeLa human cancer lines, *Inorg. Chem. Commu*, 44, (2014), 159-163.
- [6] M. Y. Jomaa, M. Altaf, S. Ahmad, A. Alhoshani, N. Baig, A-N. K. G. Bhatia, J. Singh, A. A. Isab. *Polyhedron*, (2017), <https://doi.org/10.1016/j.poly.2017.12.016>
- [7] F. Z. Boudjenane, F. T. Baara, N. Boukabcha, N. E. H. Belkafouf, N. Dege, M. Saidj, N. Khelloul, A. Djafri, A. Chouaih, Synthesis, crystallographic and spectroscopic investigation, chemical reactivity, hyperpolarizabilities and in silico molecular docking study of (Z)-2N-(tert-butylimino)-3N²-(4-methoxyphenyl)thiazolidin-4-one, *Journal of Molecular Structure*, 1287, (2023), <https://doi.org/10.1016/j.molstruc.2023.135620>.

- [8] C. Tabti, A. Benmohammed, N. Boukabcha, N. Dege, A. Djafri, F. Z. Boudjenane, A. Chouaih & A. Djafri, Synthesis, Structural Characterization and Theoretical NLO Activity of N-(4-Acetyl-5-(4-(Nitro)Phenyl)-4,5-Dihydro-1,3,4-Thiadiazol-2-yl)-N-Phenyl Acetamide, Polycyclic Aromatic Compounds, <https://doi.org/10.1080/10406638.2022.2158882>.
- [9] A. A. Isab, S. Ahmad, M. Arab, Synthesis of silver (I) complexes of thiones and their characterization by ¹³C, ¹⁵N and ¹⁰⁷Ag NMR spectroscopy, *Polyhedron*, 21, (2002), 1267–1271.
- [10] D. M. Adam, J. B. Cornell, Metal–sulfur vibrations. Part I. Far-infrared spectra of some complexes of thiourea and ethylenethiourea (imidazolidine-2-thione), *J. Chem. Soc.*, (1967), 884 – 889. <https://doi.org/10.1039/J19670000884>
- [11] B. Kosar, C. Albayrak, Spectroscopic investigations and quantum chemical computational study of (E)-4-methoxy-2-[(p-tolylimino) methyl] phenol *Spectrochim. Acta*, 78A, (2011), 160-167. <https://doi.org/10.1016/j.saa.2010.09.016>
- [12] B. J. Powell, T. Baruah, N. Bernstein, K. Brake, R. H. McKenzie, P. Meredith, M. R. Pederson, A first-principles density-functional calculation of the electronic and vibrational structure of the key melanin monomers, *J. Chem. Phys.*, 120, (2004), 8608. <https://doi.org/10.1063/1.1690758>
- [13] A. S. Faihan, R. H. AlShammari, M. Ashfaq, S. Muhammad, S. A. Al-Jibori, M. N. Tahir, M. R. Hatshan, A. S. Al-Janabi, S. M. Al-Moayid, Synthesis, spectroscopic, crystallographic, quantum and molecular docking investigations of cis-4,5-diphenylimidazolidine-2-thione, *Journal of Molecular Structure*, 1286, (2023), <https://doi.org/10.1016/j.molstruc>.
- [14] S. Alturk, N. Boukabcha, N. Benhalima, O. Tamer, A. Chouaih, D. Avcı, Y. Atalay, F. Hamzaoui, Conformational, spectroscopic and nonlinear optical investigations on 1-(4-chlorophenyl)-3-(4 chlorophenyl)-2-propen-1-one: a DFT study, *Indian J. Phys.* 91 (5), (2017), 501–511, <https://doi.org/10.1007/s12648-016-0945-3>.
- [15] N. M. O'boyle, A. L. Tenderholt, K. M. Langner, CCLIB: a library for package independent computational chemistry algorithms, *J. Comput. Chem.* 29 (5), (2008), 839–845, <https://doi.org/10.1002/jcc.20823>.
- [16] G. Angajala, V. Aruna, P. Pavan kumar, P. G. Reddy, Biocatalytic one pot three component approach: facile synthesis, characterization, molecular modeling and hypoglycemic studies of new thiazolidinedione festooned quinoline analogues catalyzed by alkaline protease from *Aspergillus niger*, *Bioorg. Chem.*, 119, (2022), 105533. <https://doi.org/10.1016/j.bioorg>.

- [17] D. Rakhmonova, L. Gapurova, S. Razzoqova, S. Kadirova, B. Torambetov, Z. Kadirova, S. Shishkina, 5-Amino-1H-benzimidazole-2(3H)-thione: molecular, crystal structure and Hirshfeld surface analysis. *Acta Cryst.* (2022), <https://doi.org/10.1107/S2056989022000792>.
- [18] V. S. Naik, P. S. Patil, N. B. Gummagol, Q. A. Wong, C. K. Quah, H. S. Jayanna, Structural, linear optical, second and third-order nonlinear optical properties of two halogenated chalcone derivatives containing thiophene moiety, *Chem. Phys. Lett.* 761, (2020), 138051, <https://doi.org/10.1016/j.cplett.2020.138051>.
- [19] N. Benhalima, N. Boukabcha, O. Tamer, A. Chouaih, D. Avci, Y. Atalay, F. Hamzaoui, Solvent effects on molecular structure, vibrational frequencies, and NLO properties of N-(2,3-dichlorophenyl)-2-nitrobenzene-sulfonamide: a density functional theory study, *Braz. J. Phys.* 46, (2016), 371–383, <https://doi.org/10.1007/s13538-016-0419-2>.
- [20] M. Dalton, E. Holzman, E. Erwin, et al, Patient navigation services for cancer care in low-and middle-income countries: A scoping review. *PLoS ONE* 14:e0223537, (2019), <https://doi.org/10.1371/journal.pone.0223537>
- [21] J. R. McIntosh, M. I. Molodtsov, F. I. Ataulakhanov, Biophysics of mitosis. *Quart Rev Biophys*, 45, (2012), 147–207. <https://doi.org/10.1017/S0033583512000017>
- [22] A. A. Samah, M. F. A. Fauzi, S. Mansor, Classification of benign and malignant tumors in histopathology images. *IEEE International Conference on Signal and Image Processing Applications (ICSIPA)*. IEEE, Kuching, (2017), pp 102–106. 23419400
- [23] M. Duffy, P. McGowan, W. Gallagher, Cancer invasion and metastasis: changing views. *J Pathol*, 214, (2008), 283–293. <https://doi.org/10.1002/path.2282>
- [24] O. D. Abaan, E. C. Polley, S. R. Davis, O. D. Abaan, E. C. Polley, S. R. Davis, Y. J. Zhu, S. Bilke, R. L. Walker, M. Pineda, Y. Gindin, Y. Jiang, W. C. Reinhold, S. L. Holbeck, R. M. Simon, J. H. Doroshov, Y. Pommier, P. S. Meltzer, The Exomes of the NCI-60 Panel: A Genomic Resource for Cancer Biology and Systems Pharmacology. *Cancer Res*, 73, (2013), 4372–4382. <https://doi.org/10.1158/0008-5472.CAN-12-3342>
- [25] J. Fazekas, T. W. Grunt, E. Jensen-Jarolim, J. Singer, Long term storage in liquid nitrogen leads to only minor phenotypic and gene expression changes in the mammary carcinoma model cell line BT474. *Oncotarget*, 8, (2017), 35076–35087. <https://doi.org/10.18632/oncotarget.16623>
- [26] S. Gomez-Ruiz, I. D. Maksimovi, S. Mijatovi, G. N. Kaluderovi, On the Discovery, Biological Effects, and Use of Cisplatin and Metallocenes in Anticancer Chemotherapy. *Bioinorg. Chem. Appl*, (2012), 1-14. <https://doi.org/10.1155/2012/140284>

- [27] V. Jaroslav, S. Jili, L. Jerzy, The influence of square planar platinum complexes on DNA base pairing. An ab initio DFT study, *Phys. Chem. Chem. Phys.*, 3, (2001), 4404-4411. <https://doi.org/10.1039/c2cp40515f>
- [28] H. Jinchuan, D. Jason, S. Aziz, A. Sheera, Cisplatin DNA damage and repair maps of the human genome at single-nucleotide resolution, *PNAS*, 113 (41), (2016), 11507-11512. <https://doi.org/10.1073/pnas.1614430113>
- [29] W. L. DeLano, Pymol: An open-source molecular graphics tool. *CCP4 Newsletter On Protein Crystallography*, 40, (2002), 82-92.
- [30] E. A. Ahmed, H. Abu Zahra, R. Ben Ammar, M. Elsayed Mohamed, H-I. M. Ibrahim. Beta-Caryophyllene Enhances the Anti-Tumor Activity of Cisplatin in Lung Cancer Cell Lines through Regulating Cell Cycle and Apoptosis Signaling Molecules. *Molecules (Basel, Switzerland)* 27, (2022), 23 8354. <https://doi.org/10.3390/molecules27238354>

General conclusion and prospects

General conclusion and prospects

This work focus on the determination of the electronic, optoelectronic, nonlinear electronic and optical properties of the two trans-[Pt(NH₃)₂(Imt)₂](NO₃)₂ and trans-[Pt(NH₃)₂(Me₂Imt)₂](NO₃)₂ compounds. The theoretical calculation using the density functional theory DFT investigate the parameter values of IR, NMR, NLO and all other parameters, and offers a cost-effective computational alternative for handling large molecules.

The outcomes of experimental spectroscopic assessments on the newly examined molecular compounds, denoted as 1 and 2, are strongly correlated with their theoretically predicted values. However, some disparities were observed in computed spectroscopic data as NMR calculation due to the absence of the DMSO solvent.

In the context of infrared vibrational spectroscopy, the differences in frequency values primarily stem from the absence of anharmonic contributions in the theoretical calculations. The molecular and electronic characteristics of these molecules are then studied using the results of a thorough structural analysis using B3LYP functional GEN and 6-311 G (d, p) basis set using the Gaussian 09 software.

The results of the method for the two complexes are very similar to those of the experimental results in bond lengths and valence angles confirming the non planarity in the geometry. The overall electronic behavior of each compound was evidenced by the reorganization energy of electrons and holes and the global reactivity indices. At the same time, the optoelectronic behaviour was determined to show that the compound 1 has a dipolar moment equal to 3.17538 Debye, polarizability α_{tot} to 35.0713×10^{-23} and 42.7482×10^{-23} esu for both complexes respectively, and a very important hyperpolarizability equal to 0.797097×10^{-30} and 4.35676×10^{-30} esu, respectively. Considering these findings, it is reasonable to classify both complexes as suitable molecules for nonlinear optics (NLO) applications.

Finally, the biological activity was studied to investigate the potential of lung cancer inhibitory effect utilizing Autodock 4.0 software. The results show a binding affinity of -5.19 and -6.40 kcal/mol for the complexes 1 and 2, respectively against the protein cyclin-dependent kinase CDK6 derived from the A549 cell denoted as 4EZ5.

In the perspective and in the continuity of this research work, it is desirable to extend and complete this work by an analysis of the toxicity of these compounds. The physicochemical study of our thione compounds is considered as a preliminary and main step to predict their

General conclusion and prospects

properties and to elaborate their functionalities. This step provides useful information for future investigations on the activity and application of both compounds (1 and 2) and paves the way for the design of new, more efficient thione molecular structures. For this, we also plan to exploit in the future the results of this thesis in the study and realization of drugs from the discovery of drugs with the biological activity that has been studied.